MINISTRY OF EDUCATION

THE ANNALS OF "DUNAREA DE JOS" UNIVERSITY OF GALATI

Fascicle IX
METALLURGY AND MATERIALS SCIENCE

YEAR XL (XLV)
June 2022, no. 2

ISSN 2668-4748; e-ISSN 2668-4756

2022
GALATI UNIVERSITY PRESS

EDITORIAL BOARD

THE ANNALS OF "DUNAREA DE JOS" UNIVERSITY OF GALATI
FASCICLE IX. METALLURGY AND MATERIALS SCIENCE
Nº. 2 - 2022, ISSN 2668-4748; e-ISSN 2668-4756
Volume DOI: https://doi.org/10.35219/mms.2022.2

Table of Contents

Nº. 2 - 2022, ISSN 2668-4748; e-ISSN 2668-4756
Volume DOI: https://doi.org/10.35219/mms.2022.2

THE ANNALS OF "DUNAREA DE JOS" UNIVERSITY OF GALATI
FASCICLE IX. METALLURGY AND MATERIALS SCIENCE
N°. 2 - 2022, ISSN 2668-4748; e-ISSN 2668-4756
Article DOI: https://doi.org/10.35219/mms.2022.2.01

THE EVOLUTION OF CO_2 EMISSIONS FROM THE HEATING SYSTEMS OF A LARGE CITY

Aura OSANU[1], Liviu ENACACHE[2], Marius BODOR[1,*]
[1] "Dunarea de Jos" University of Galati, Romania
[2] S.C. CALORGAL S.A., Galati, Romania
e-mail: marius.bodor@ugal.ro

ABSTRACT

Different current reasons, like global warming due to greenhouse gases and high energy prices, creates the necessity to make the heating systems in large cities more efficient. The present paper presents a real situation for an urban agglomeration, regarding the transition from a centralized heating system to a decentralized one. Two types of decentralized possibilities are discussed and analyzed taking into account especially the CO_2 emissions, during several recent years. In this respect, a calculus of CO_2 emissions from the former heating system, compared to the present heating systems is also presented and discussed.

KEYWORDS: heating systems, CO_2 emissions, pollution

1. Introduction

The world is moving towards the least favorable scenario estimated by the Intergovernmental Panel on Climate Change (IPCC), leading to a significant possibility of overheating by 4 °C by the end of this century. In order to meet the global carbon budget needed to limit global warming to 2 °C, the global economy needs to increase its decarbonization level to 6.2% per year by 2100, which would ensure that virtually the global energy system will have zero carbon emissions by the end of the century [1].

Also, it is expected that by 2050, national and international measures to reduce fossil fuel consumption will become a possibility and a necessity that is hard to ignore. The first phase of climate change will result in a 4 °C increase in global average temperature, which could happen in the next 30-50 years. Even if the measures discussed above were taken immediately, it would be very likely that this change in average temperature would take place in the next 50 years [2].

But a second phase of climate change, namely a 2 to 3 °C increase in average temperature, which would mean an increase of 4 to 6 °C in temperate climates and even greater changes in the polar regions - is an evolution on which the world will probably decide to at least postpone it as much as possible. Clearly, a small increase or stabilization in global fossil fuel consumption would slow down the global warming trend, which would greatly increase humanity's chances of developing a sound policy to adapt to the effects of climate change [3].

We can therefore assume that this possible change in the Earth's climate would have detrimental effects in certain regions without, however, constituting a catastrophic evolution for all mankind. It could lead to changes in agricultural activity and trade balances, as well as in the way of life of many people, and eventually, in a few centuries, it would lead to the evacuation of lowland areas as a result of the considerable increase of ocean water level. Avoiding or at least postponing these adverse effects is an ideal based on the hope that the countries of the world will eventually launch a joint effort to limit the consumption of fossil fuels [4].

Carbon dioxide (CO_2) is one of the most dangerous greenhouse gases because it can stay in the atmosphere for hundreds of years. This is due, among other things, to the burning of fossil fuels, on which we have become very dependent in industry, energy and transport. It is estimated that since the Industrial Revolution, the concentration of carbon dioxide in the atmosphere has increased by 43% [5].

Globally, warming in the Arctic is thought to be associated with less extreme cold weather in the northern hemisphere, and climate change will lead to moderate winters in Europe and the United States. Scientific results show that warming of 0.1 °C/decade is expected in the next two decades, even if the concentration of all greenhouse gases and aerosols remains constant in 2000 [6].

THE ANNALS OF "DUNAREA DE JOS" UNIVERSITY OF GALATI
FASCICLE IX. METALLURGY AND MATERIALS SCIENCE
N°. 2 - 2022, ISSN 2668-4748; e-ISSN 2668-4756
Article DOI: https://doi.org/10.35219/mms.2022.2.01

In response, local, national, regional and international initiatives are being developed and implemented to limit greenhouse gases (GHG) concentrations in the Earth's atmosphere. Such GHG initiatives are based on quantifying, monitoring, reporting and verifying GHG emissions. With regard to reducing the impact of climate change, the key factor is the policies to meet the EU's 2030 commitments to reduce GHG emissions by at least 40% from 1990 levels and a 27% improvement of energy efficiency [7].

Since wind and solar energy are variable resources and do not yet provide capacity commitments for peak load, increasing their penetration will require a complementary capacity for peak load [8].

In support of the goals described above, the energy efficiency of heat supply systems can be a real help. In the case of Romania, in order to rehabilitate the centralized heat supply systems of some localities, the works performed contributed to the increase of energy efficiency, by streamlining the centralized systems of production, transport and distribution of thermal energy and to increase the quality of the public heat supply service.

In order to support efforts to reduce greenhouse gas emissions and thus limit global warming, accurate information is needed on emission levels, developments and policies and measures to improve the situation. To this end, a sound framework for monitoring and reporting GHG emissions is needed, as well as reliable information on the changes that existing and planned policies and measures are expected to bring about in terms of emissions.

Regarding Romania, CO_2 emissions from different sectors of activity also highlight the major contribution of the energy sector and transport, which means that these are the areas on which it is necessary to implement measures and actions to reduce CO_2 emissions.

The case study in this paper is related to the centralized system for thermal energy supply (SACET) in the city of Galați, Romania. Currently this system supplies thermal energy to about 6000 apartments and 17 public institutions, economic agents and has the following main components: i) source of thermal energy production (natural gas boilers, installed in 24 thermal points); ii) the primary circuits that ensure the closed circuit of the thermal energy between the source, the hot water boilers and the heat exchangers from the thermal points; iii) the secondary thermal networks that ensure the distribution of thermal energy from the thermal points to the final consumers and iv) final consumers. GHG from this centralized system is compared with individual heating (IH) systems used by a large part of population of Galati municipality.

In 1990, the central heating system of Galati municipality was connected to approx. 90,000 apartments and the heating agent was procured from a now defunct Combined Heat and Power Unit (CHPU), located outside the city, on a nearby metallurgical complex platform. Taking into account the large number of disconnections and the technical-economic inefficiency of the former central heating system, the authorities of Galați municipality, started in 2017 two parallel programs aiming the following: i) installation of heating capacities in all schools and ii) providing the population with financial aid for alternative heating resources. These directions were in line with the idea, also stated in [9], that a particular heating system could be favored for its efficiency but mostly for its cost.

In March 2018, only a number of 18,366 apartments were still connected to the system, which led the local authorities to abandon the old centralized system and reorganize another one. Also, as a result of this decision, another 7,844 IH systems, on natural gas, of 24 kW, were installed, with a total power of 188.256 MW. The statistical data show that before this organized decentralization, there were already a number of about 29,000 IH systems installed in the city.

The priority given to the efficiency of the present SACET configuration results from the following advantages: i) fuel economy; ii) reduction of air pollution; iii) the promotion/expansion of modern, state-of-the-art systems meeting the general needs of increasing energy efficiency and environmental protection.

Based on historical data on the configuration of heating systems in the city of Galați, Romania and the method of calculating carbon dioxide emissions from these systems, this paper has managed to highlight the evolution over time of CO_2 emissions; the differences (regarding the CO_2 emissions) between the mentioned heating systems were identified and also, diminishing the impact on the environment by replacing and/or modifying the old heating system was emphasized.

2. Methodology

The price trend of the heating agent is subject to continuous increase due to the exchange rate, the price of fuels and other factors that determine the price adjustment. To these factors are added the external environmental costs. In the face of inevitable increases, it is necessary for the thermal energy supplied from the centralized systems to enter into fair competition with other solutions.

The continuous increase in the rate of disconnection from the centralized system was determined, on the one hand, by the poor quality of the service provided and the high price, and on the

THE ANNALS OF "DUNAREA DE JOS" UNIVERSITY OF GALATI
FASCICLE IX. METALLURGY AND MATERIALS SCIENCE
Nº. 2 - 2022, ISSN 2668-4748; e-ISSN 2668-4756
Article DOI: https://doi.org/10.35219/mms.2022.2.01

other hand by the low price of natural gas offered to captive consumers through subsidy mechanisms. Thus, reducing the phenomenon of disconnections and possibly the return of disconnected consumers to the centralized system will not be possible without adopting a viable alternative solution to IH systems, and this solution can only be the low price of the central heating system.

Knowledge regarding the combustion mechanisms of fuels is very important in the regulation and operation of thermal equipment, so that they work with complete combustion, in designed parameters and with maximum efficiency, essential elements in reducing energy consumption and, implicitly, with optimal results in terms of GHG emissions. In this sense, we can say that the combustion reaction of methane is the following:

$$CH_4 + 2O_2 \rightarrow CO_2 + 2H_2O \quad (1)$$

$$1\ kmol\ CH_4 + 2\ kmol\ O_2 \rightarrow 1\ kmol\ CO_2 + 2\ kmol\ H_2O \quad (2)$$

Carbon dioxide emissions can be determined by direct measurements, with specific equipment, or by calculation. For optimal monitoring of GHG emissions it is necessary to define the calculation parameters, which can be implicit or determined by analysis [10]. The calculation of GHG emissions is made according to Regulation (EU) no. 601 of 21 June 2012 on the monitoring and reporting of GHG emissions in accordance with Directive 2003/87/EC [11].

In the present study, the calculations are based on the following variables:

- activity data, meaning the amount of fuel or materials consumed or produced by a process, relevant to the calculation-based monitoring methodology, expressed in terajoules, tones per mass or, for gases as normal volume in cubic meters (explanation of calculation: for example, the consumption of 479,594 m^3 of gas is converted from m^3 to Nmc according to the relation: 479,594 m^3 x 273.15/288.15 = 454,628.15 Nmc);
- net calorific value (NCV), meaning the specific amount of energy released in the form of heat when a fuel or material is subjected to a complete process of combustion with oxygen under standard conditions, without taking into account the heat water vaporization possibly formed (the value is considered a constant equal to 0.00003658 [TJ/Nmc]);
- emission factor (FE), meaning the average rate of emission of a GHG relative to the activity data of a source stream assuming complete oxidation in the case of combustion and full conversion for all other chemical reactions (the value is considered a constant equal to 55.61 [tCO_2/TJ]);
- oxidation factor (OF), meaning the ratio of carbon oxidized to CO_2 as a result of combustion to the total carbon content of the fuel, expressed as a fraction, of carbon monoxide (CO) emitted into the atmosphere as the equivalent molar amount of CO_2 (the value is considered a constant without a measuring unit, equal to 1).

Thus, the formula used in CO_2 emissions calculation for this study is the following:

$$CO_2\ emissions\ [tCO_2] = Gas\ consumption\ [Nmc] \times NCV\ [TJ/Nmc] \times FE\ [tCO_2/TJ] \times FO \quad (3)$$

The NCV and FE values are taken from the List of national values of net emission factors and calorific values, specific to each fuel type and activity category, used to meet the requirements for monitoring and reporting carbon dioxide emissions. The values in this list apply to small combustion plants [12].

This calculation method shows that the total value of CO_2 emissions is directly proportional to the gas consumption of combustion plants. So, for the calculation of the quantities of CO_2 emitted, we need to highlight the natural gas consumption of all heating systems.

3. Results and discussions

3.1. Evolution of CO_2 emission values of the former centralized heating system

Using the gas consumption data for the former CHPU during the 2013-2017 period, we can make an analysis based on calculation of the GHG emissions generated (Figure 1). Year 2017 was the last one with this former unit suppling thermal energy for SACET Galați.

THE ANNALS OF "DUNAREA DE JOS" UNIVERSITY OF GALATI
FASCICLE IX. METALLURGY AND MATERIALS SCIENCE
No. 2 - 2022, ISSN 2668-4748; e-ISSN 2668-4756
Article DOI: https://doi.org/10.35219/mms.2022.2.01

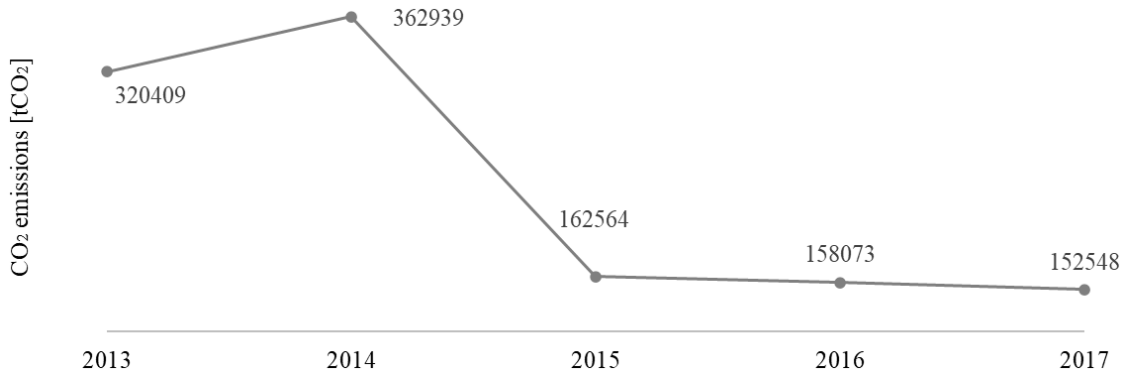

Fig. 1. *Evolution of calculated CO_2 emissions, during 2013-2017, from the Combined Heat and Power Unit responsible with the thermal energy supplied to SACET Galați*

Thus, we observe a consistent decrease in gas consumption from 166,159,727 cubic meters of gas in 2013 to 79,762,203 cubic meters of gas in 2017 and, implicitly, in greenhouse gas emissions from 320,409 tons of CO_2 in 2013 to 152,548 tons of CO_2, so a decrease of more than 50%. This decrease was generated starting with year 2105 by the decrease in heat demand and mass disconnection of consumers, that compelled the CHPU to function seasonally accordingly to the existing demand of thermal energy.

The age of heat transferring networks lead to massive losses, which were translated into additional costs to be covered by a decreasing number of consumers. Thus, the public district heating service became much too expensive compared to other technologies for supplying thermal energy. All these elements resulted in massive disconnections from the municipal district heating system. Thus, many citizens have installed IH systems. This transition resulted in a drastic reduction of CO_2 emissions, as already stated, but unfortunately, also in transferring the remaining emissions from outside the city to the heavily populated areas.

3.2. Evolution of CO_2 emission values of the present heating systems

By adding up the CO_2 emissions generated by SACET, heating systems of new apartment buildings (ANL), sports complexes and schools, a clear view is possible regarding the evolution of CO_2 emissions throughout an entire year. Since most of the thermal power generation units operate seasonally, with a peak load during the cold season, it is noticed that the major share of CO_2 emissions is recorded in January, February, March, April, November, and December (Figure 2).

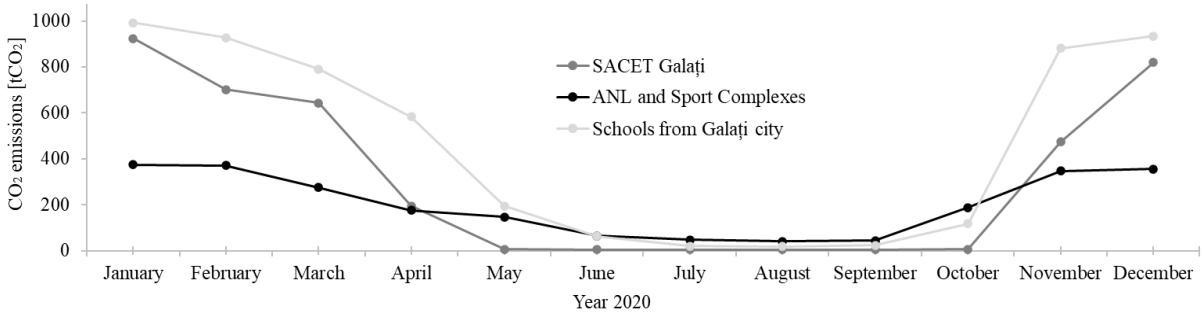

Fig. 2. *Evolution throughout year 2020 of CO_2 emissions from SACET, heating systems of new apartment buildings (ANL), sports complexes and schools in Galați city*

For this study, it was not possible to accurately quantify the consumption of each apartment. Nevertheless, by using the data from the natural gas distribution operator for the municipality of Galați, in 2020, strictly for household consumers, a natural gas consumption of 28,585,000 m^3 was registered. This data was then used to obtain the CO_2 emissions resulted from IH systems utilization in Galați city. In this respect, Figure 3 presents these CO_2 emissions compared to the above values of other CO_2 emission sources and also the cumulated CO_2 emitted in Galați city in 2020 from all types of heating systems.

THE ANNALS OF "DUNAREA DE JOS" UNIVERSITY OF GALATI
FASCICLE IX. METALLURGY AND MATERIALS SCIENCE
No. 2 - 2022, ISSN 2668-4748; e-ISSN 2668-4756
Article DOI: https://doi.org/10.35219/mms.2022.2.01

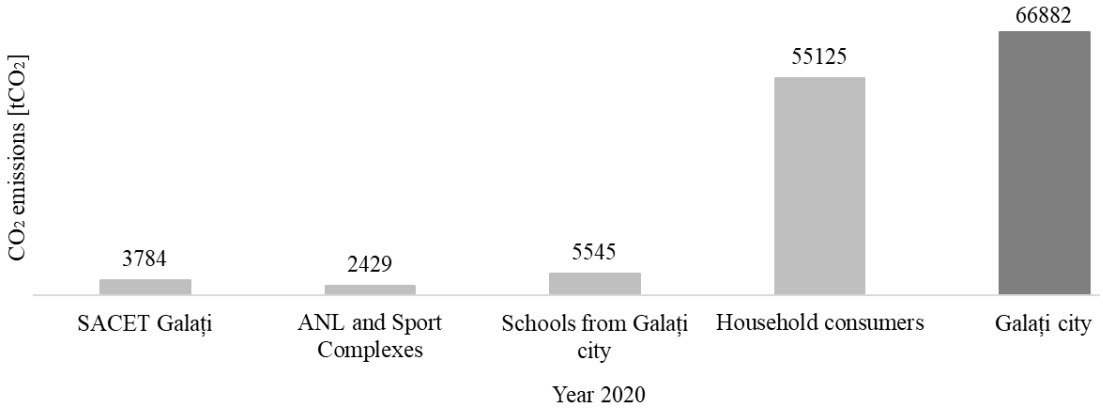

Fig. 3. *Evolution of CO_2 emissions from all types of heating systems in Galați city during the year 2020*

The cumulated CO_2 emissions in 2020 in Galați city from all heating sources present the largest contribution from the household consumers (55,125 m^3). However, this amount is less than half the quantity registered for the last year (2017) of CHPU operation, totaling 152,548 m^3 of CO_2 emissions for this unit alone.

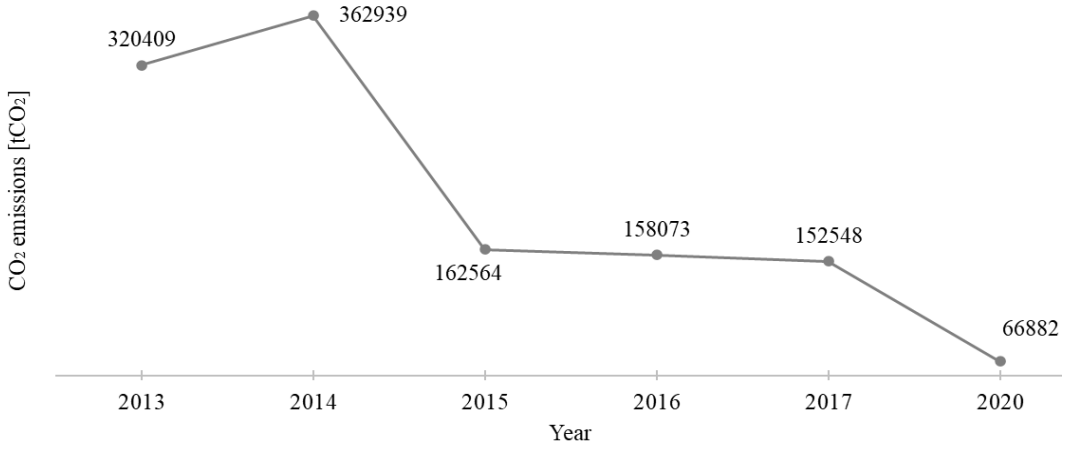

Fig. 4. *Evolution of CO_2 emissions from CHPU during the 2013-2017 period compared to CO_2 emissions from all heating systems in Galați city during the year 2020*

This comparison is better placed in perspective by completing Figure 1 with the latest data presented earlier. Thus, Figure 4 presents the evolution of CO_2 emissions from CHPU during the 2013-2017 period, compared with CO_2 emissions from all heating systems in Galați city in 2020. This big difference of CO_2 emission values throughout these years is based on multiple reasons, the most influential being supposed to be the increase in gas price and replacing outdated heating systems with new ones.

4. Conclusions

Reiterating the formula for calculating CO_2 emissions, in order to reduce emissions, one can intervene on a single variable, namely the consumption of natural gas. In some cases, the transmission networks of the thermal agent operate with low efficiency, high specific consumptions, a situation that is due primarily to the advanced physical and moral wear of the existing pipes. The average heat loss was sometimes nearly 28%, especially for the old heating system in Galați city. All this is reflected in high consumption of natural gas and electricity, which leads to unreasonable production costs for heating systems. Apart from the state of the thermal networks, another element that leads to increased natural gas consumption is the improper operation of the systems.

THE ANNALS OF "DUNAREA DE JOS" UNIVERSITY OF GALATI
FASCICLE IX. METALLURGY AND MATERIALS SCIENCE
N°. 2 - 2022, ISSN 2668-4748; e-ISSN 2668-4756
Article DOI: https://doi.org/10.35219/mms.2022.2.01

Some proposed measures to increase the energy efficiency of the district heating system and thus to reduce energy consumption and CO_2 emissions are the following: i) resizing and replacement of secondary thermal energy transmission networks with pre-insulated steel pipes. The need to resize the networks results from the fact that these thermal power plants serve a smaller number of consumers than originally proposed; ii) rehabilitation of non-modernized thermal points; iii) reduction of the massive losses of the addition water by counting the final consumers on the heating circuits; iv) automation and monitoring of all heating systems.

In order for heating systems to produce thermal energy to operate in optimal parameters, with low gas and electricity consumption, another element is the quality of natural gas. Thus, in July 2020, an analysis laboratory with national accreditation was requested to perform chromatographic analyzes on the quality and chemical composition of the gas used by SACET.

Another measure that is recommended to reduce natural gas consumption is thermal insulation of all buildings that benefit from any heating system reliant on natural gas.

The adoption of the above-mentioned measures would lead to a significant increase in the efficiency of the systems and a reduction of about 25% in natural gas consumption and, implicitly, in CO_2 emissions.

Until all GHG emissions will fall towards targeted values, their monitoring will have to be maintained or even made more effective in the future. These data will continue to offer important information regarding the necessity to optimize all types of heating systems, with direct impact on the overall emissions and also the price of heating commodities.

References

[1]. ***, https://ec.europa.eu/clima/change/causes_roș.
[2]. Umid Abuzarli, Laman Mammadzada, *Opțiuni strategice pentru reducerea emisiilor de gaze cu efect de seră în diferite sectoare ale activității economice*, ASE București, 2014.
[3]. Ardelean F., Colda I., *Cauzele schimbărilor climatice - un subiect controversat*, Conferința a XV-a Eficiență, Confort, Conservarea Energiei și Protecția Mediului, Facultatea de Instalații, București, 2008.
[4]. ***, https://documentar25.wordpress.com/2016/04/13/omul-si-clima-efectul-de-seră.
[5]. ***, Climate Adapt – *Platforma europeană pentru adaptarea la schimbările climatice pentru România*, http://climate-adapt.eea.europa.eu/countries/romania.
[6]. ***, *Schimbările climatice și mediul construit din România*, http://www.ecceengineers.eu/news/files/Climate_change_romania.
[7]. ***, MEWT, *Cea de-a treia comunicare a României privind schimbările climatice* în cadrul Convenției cadru a Organizației Națiunilor Unite asupra schimbărilor climatice, 2005.
[8]. ***, *Starea Actuala a Sistemelor Centralizate de Termoficare – Propuneri pentru Reabilitarea și Dezvoltarea Acestora*, Cogen România, 2011.
[9]. Taeyeon Yoon, Yongsun Ma, Charles Rhodes, *Individual heating systems vs. district heating systems: what will consumers pay for convenience*?, Energy Policy, 86, p. 73-81, 2015.
[10]. ***, SR EN ISO 14064-1:2019, *Gaze cu efect de seră. Partea 1: Specificații și ghid, la nivel de organizație, pentru cuantificarea și raportarea emisiilor și a cantităților îndepărtate de gaze cu efect de seră*.
[11]. ***, *Regulamentul (UE) nr. 601/2012 al Comisiei din 21 iunie 2012 privind monitorizarea și raportarea emisiilor de gaze cu efect de seră în conformitate cu Directiva 2003/87/CE* a Parlamentului European și a Consiliului.
[12]. ***, *Lista privind valorile naționale ale factorilor de emisie și ale puterilor calorifice nete, specifice fiecărui tip de combustibil și categorie de activitate*.

THE ANNALS OF "DUNAREA DE JOS" UNIVERSITY OF GALATI
FASCICLE IX. METALLURGY AND MATERIALS SCIENCE
N°. 2 - 2022, ISSN 2668-4748; e-ISSN 2668-4756
Article DOI: https://doi.org/10.35219/mms.2022.2.02

AN INTERACTIVE METHOD FOR CALCULATING THE MAXIMUM EFFICIENCY (ORGANIC YIELD) IN THE PROCESSING OF THE TAILING DUMPS IN JIU VALLEY

Mihaela Olga MARIȚA[1], Viorica CIOCAN[2], Ildiko BRÎNAȘ[3]*
[1]PhD student, University of Petroșani, Petroșani, Romania
[2]Researcher I, R&D National Institute for Metals and Radioactive Resources - ICPMRR, Bucharest, Romania
[3]Lecturer, University of Petroșani, Petroșani, Romania
e-mail: mihaela_marita98@yahoo.com, kerteszildiko@ymail.com

ABSTRACT

The interactive method presented in the paper, allows the calculation of maximum efficiency indicators (organic yields) of the processing and operational control of the actual processing process. It also allows the correlation of the technological parameters with the economic ones in order to properly capitalize on the products obtained by processing a material (raw coal or sterile resulted from coal preparation) containing solid fuel fractions. Using the interactive system, one can pre-determine the optimal mixture of material to be processed and have different characteristics. The interactive method consists of three C programs that allow: the selection of the mixture of solid material to be processed, by tracing the abacuses and determining the theoretical weight extractions, depending on the desired quality of the concentrates; calculation of the organic processing yields; estimating the processing results, using the Fournol method, taking into account the performance of the processing equipment used and the density of separation between the products.

KEYWORDS: efficiency indicators, coal processing, interactive system, tailings dump, Fournol method

1. Introduction

Although the coal extraction and processing activities have diminished a lot in Romania as a result of restructuring the mining activity, it is still necessary to study the processing in terms of efficiency, given the large reserves of fuel mass that exist both in the underground coal deposits, as well as in the tailings dumps across the Jiu Valley.

For an operational leading of a coal processing activity, it is necessary to know the maximal technological parameters and therefore it was proposed an interactive system for substantiating and determining the maximum coal processing efficiency.

The importance of elaborating a novel scientific methodology, resides in the need of reducing the degree of energy dependence on other states in the region, due to current political and economic points of view.

The interactive system consists of a three computer programs package which allows calculating rapidly the coal processing efficiency. The proposed methodology replaces the classical method of abacuses reading in order to establish the theoretical recovery value and thus, the efficiency.

The new method uses only the same data bases of the densimetric analysis on granulometric classes, which allows the abacuses tracing [1] in order to calculate the theoretical recoveries.

The three programs elaborated in C [2], allow:

- The selection of coal collieries which feeds the coal plant in order to establish a global densimetric analysis on a mixture of coals;
- The calculus and the tracing of washing curves HR for the coals mixture and for any ash content of the feeding;
- The calculus of the maximal recoveries, taking into account not only the densimetric analysis but also the selectivity indices of the concentration installations and the separation density between products. No matter what the calculus methodology is, in the coal processing plants, it is usually applied the notion of "organic efficiency":

THE ANNALS OF "DUNAREA DE JOS" UNIVERSITY OF GALATI
FASCICLE IX. METALLURGY AND MATERIALS SCIENCE
N°. 2 - 2022, ISSN 2668-4748; e-ISSN 2668-4756
Article DOI: https://doi.org/10.35219/mms.2022.2.02

$$\eta = \frac{v_r}{v_t} \cdot 100 \quad (1)$$

Briefly, the new methodology consists of the recalculation of a densimetric analysis on a coals blend, the washing curves tracing for any ash content (to determine the theoretical recovery v_t) and the calculus by the Fournol method of the possible recovery, v_r [3, 4].

2. The Interactive System Description and Program Results

For a proper assessment of the coal processing results, it is necessary to know the densimetric analysis of the rough coal.

A different washability of coals from different zones influences the selectivity indices of concentration machines. Therefore, the establishment of an average densimetric analysis from a blend of coals is an important step of the proposed interactive system. This densimetric analysis is the data base for starting the global calculus and these are carried out for different periods of time; the samples are representative in time and this is also an important aspect of our research. The selectivity of coal processing is different on granulometric classes and that's why the densimetric analysis and the calculus stages are carried out on two granulometric classes which represent the concentration installations feeding. In order to establish a global densimetric analysis for a coals mixture, it is necessary to know the coal-classes weight and their ash content. In this way it will be possible to recompose the granulometric and densimetric composition of the plant's feeding by a successive weighting average.

The SELECT program allows to do this calculus, starting from a selection matrix of the coal colliery (A) and from two matrices which include the densimetric analysis results on granulometric classes (B) and (C) - the last matrices with the same form. The general format of these matrices is presented in Tables 1, 2 and 3 [5, 6].

Table 1. *Matrix A*

Mines / Coal plant	**P_1**	**P_2**	**P_3…**	**P_n**
E_1	1	0	1	1
E_2	1	0	0	1
E_3	0	1	0	1
E_4…	0	1	1	0
E_n	0	1	0	0

Table 2. *The form of matrices B and C*

Densimetric fractions, t/m³											
-1.4		**1.4-1.5**		**1.5-1.7**		**1.7-1.9**		**1.9-2.0**		**+2.0**	
v^*	y^{**}	v	y	v	y	v	y	v	y	v	y
v_{11}	y_{11}	v_{12}	y_{12}	v_{13}	y_{13}	v_{14}	y_{14}	v_{15}	y_{15}	v_{16}	y_{16}
v_{21}	y_{21}	v_{22}	y_{22}	v_{23}	y_{23}	v_{24}	y_{24}	v_{25}	y_{25}	v_{26}	y_{26}
v_{31}	y_{31}	v_{32}	y_{32}	v_{33}	y_{33}	v_{34}	y_{34}	v_{35}	y_{35}	v_{36}	y_{36}
v_{41}	y_{41}	v_{42}	y_{42}	v_{43}	y_{43}	v_{44}	y_{44}	v_{45}	y_{45}	v_{46}	y_{46}
…	…	…	…	…	…	…	…	…	…	…	…
v_{n1}	y_{n1}	v_{n2}	y_{n2}	v_{n3}	y_{n3}	v_{n4}	y_{n4}	v_{n5}	y_{n5}	v_{n6}	y_{n6}

* - weight recovery, % ** - ash contents, %

The HR program makes up the basis of the abacuses tracing, in order to establish the theoretical recovery. The abacuses are graphic representations of the quantity and the quality variation of the concentrate with the ash content of the rough coal (the feeding) [7].

The abacuses tracing is possible only if we consider that, in time, the washability of coal is constant; this assumption allows the HR curves tracing for any ash content in the plant feeding.

The calculus algorithm is very simple: maintaining constant the ash contents on densimetric fractions, we recalculate the weight recoveries (the quantities), by applying a correction coefficient, calculated by the relation:

THE ANNALS OF "DUNAREA DE JOS" UNIVERSITY OF GALATI
FASCICLE IX. METALLURGY AND MATERIALS SCIENCE
No. 2 - 2022, ISSN 2668-4748; e-ISSN 2668-4756
Article DOI: https://doi.org/10.35219/mms.2022.2.02

$$k = \frac{v_1}{v_2} \quad (2)$$

- v_1 represents the concentrate weight recovery (all the densimetric fractions under the density 1.9 kg/dm^3) for the initial ash content of the coal plant feeding;

- v_2 is the concentrate weight recovery for an imposed ash content (the new content for what we desire to recalculate and to trace the HR curves);

The value of v_2 is calculated by the relation:

$$v_2 = \frac{b-a}{b-c} \cdot 100 \quad (3)$$

where:

b - is the ash content of the densimetric fraction +1.9 kg/dm^3;

a - represents the imposed average ash content (for the new HR curves);

c - the ash content of the concentrate (weighting average of ash contents of densimetric fractions = 1.9 kg/dm^3 from the densimetric analysis).

The correction coefficient k, can be under or over unitary, depending on the imposed ash content.

Applying this calculus algorithm, we can trace un unlimited number of washability curves, in order to obtain a high accuracy of the abacuses. We can establish directly the theoretical recoveries for any ash content of the rough coal and of the concentrate, by abacuses reading.

The automatically calculated data, which is the basis for the HR curves tracing are presented in Table 3.

The computer HR curves are rendered in Figure 1 and the abacuses resulted from the HR curves interpretations are presented in Figure 2.

Table 3. *The computer data for the HR curves*

δ	DATE ANALIZE v (%)	y (%)	Σv +v/2 (%)	Σv (%)	'c' v·y	Σv·y	Σv·y/Σv	'b' 100-Σv	100a-Σvy	100a-Σvy /100a-Σv
								100.00	5000.00	50.00
-1,4	7.47	6.12	3.73	7.47	45.71	45.71	6.11	92.53	4954.28	53.54
1,4-1,5	14.25	12.10	14.59	21.72	172.42	218.14	10.04	78.28	4781.85	61.08
1,5-1,7	11.98	22.90	27.71	33.70	274.34	492.48	14.61	66.30	4507.51	67.98
1,7-1,9	11.27	32.80	39.33	44.97	369.65	862.13	19.17	55.03	4137.86	75.19
1,9-2,0	7.39	46.10	48.66	52.36	340.67	1202.81	22.97	47.64	3797.18	79.70
+2,0	47.64	78.50	76.18	100.00	3739.74	4942.55	50.00	0.00	0.00	

Copie ecran?(D/N)
Preselectie=↑↓→,Selectie=↵,Remunt=Esc Univ.din Petrosani

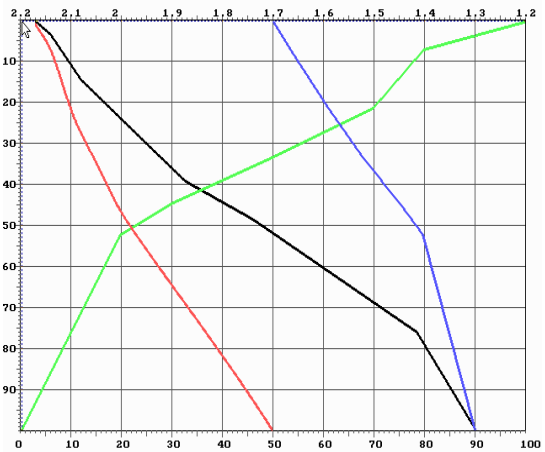

Fig. 1. *The washability curves HR*

THE ANNALS OF "DUNAREA DE JOS" UNIVERSITY OF GALATI
FASCICLE IX. METALLURGY AND MATERIALS SCIENCE
No. 2 - 2022, ISSN 2668-4748; e-ISSN 2668-4756
Article DOI: https://doi.org/10.35219/mms.2022.2.02

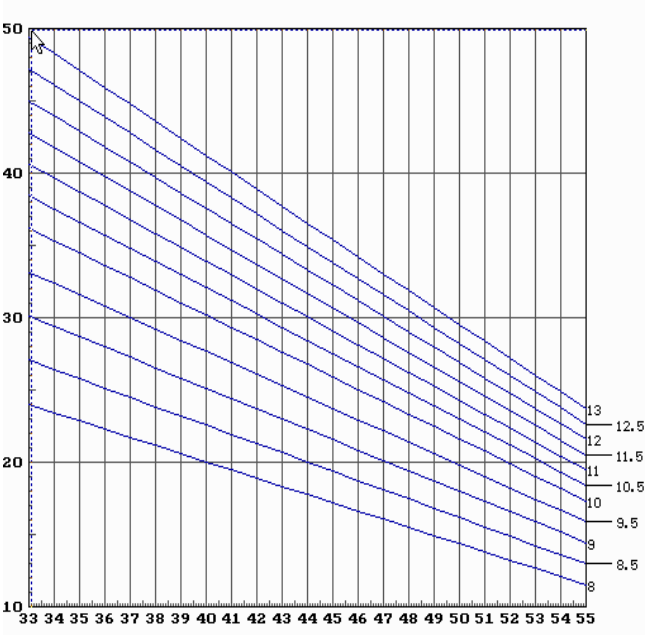

Fig. 2. *The abacuses of the theoretical recovery variation with the ash content from the rough coal and from the concentrate*

To establish the probable recovery, we used the mathematical method of Fournol, starting from the densimetric analysis, the concentration machine imperfection and the separation density. The results obtained by using the FOURNOL program are presented in Table 4.

Table 4. *The computer results from the Fournol method*

dm	Brut			x	n				
	vi(%)	yi(%)	vi*yi			ci=vi*n	ki=viyi*n	vi-ci	vi*yi-ki
1.35	1.96	6.12	12.00	2.6108	0.9954	1.9526	11.9502	0.0088	0.0542
1.45	8.17	12.10	98.87	1.6642	0.9519	7.7788	94.1240	0.3926	4.7506
1.60	9.58	22.90	219.41	0.5806	0.7194	6.8930	157.8511	2.6884	61.5653
1.80	9.57	32.80	314.11	-0.5029	0.3075	2.9449	96.5943	6.6316	217.5168
1.95	6.30	46.10	290.72	-1.1502	0.1250	0.7888	36.3672	5.5175	254.3604
2.10	55.28	78.50	4339.96	-1.7024	0.0442	2.4487	192.2259	52.8374	4147.7382
			5275.09			22.8071	589.1130	68.0765	4685.9858
							25.8302		68.8340

Copie ecran?(D/N)
Preselectie=↑↓→,Selectie=◄┘,Renunt=Esc Univ.din Petrosani

The comparative results between the coal efficiencies planned, realized in the processing plants over time, and calculated by the interactive system, are presented in Table 5.

THE ANNALS OF "DUNAREA DE JOS" UNIVERSITY OF GALATI
FASCICLE IX. METALLURGY AND MATERIALS SCIENCE
No. 2 - 2022, ISSN 2668-4748; e-ISSN 2668-4756
Article DOI: https://doi.org/10.35219/mms.2022.2.02

Table 5. *The comparative results of the coal processing efficiencies*

Coking coal efficiency, %			Global efficiency, %		
Planned	**Real**	**IS calculus**	**Planned**	**Real**	**IS calculus**
70	59.1	60.2	85	87.7	87.0
70	54.9	58.3	85	86.5	86.9
70	48.7	56.8	85	87.9	85.7
70	46.2	57.0	85	84.0	85.1
70	45.5	55.4	85	83.8	84.3
70	42.7	48.3	85	81.7	84.5
70	29.2	49.2	85	79.3	83.9
70	28.3	48.7	85	78.4	84.0
70	23.4	50.2	85	72.8	83.5
70	17.9	49.6	85	74.5	83.6

The data interpretation emphasizes some aspects e.g.:

- the differences between the classical and the new methodology of calculating the coal processing efficiency are acceptable, on the conditions of using the abacuses tracing;
- for the global efficiency, the planned and the calculated values by the proposed system are very closed, but it's obviously that the planned values must be modified in time, depending on the feeding quality.

3. Conclusions

The interactive system for substantiating and determining the maximum coal efficiency allows:

The interactive method for calculating the maximum efficiency (organic processing yields) of a solid raw material containing a mass of fuel in the form of coal, allows:

- the efficiency calculus by eliminating the classic method where the theoretical recovery (the weight concentrate extraction) is determined by reading on the abacuses;
- the establishment of maximal efficiencies values possible to achieve for any coals blend (with the same or with different washability) in correlation with the market demands;
- the calculus of the optimal values of the separation efficiencies on granulometric classes in order to obtain an automatic adjustment of the concentration machines (especially of the jigging machines); for the jigging process we have a rapid method to establish the efficiency criterion which include the separation between the three concentration products (the coking coal, the energetic coal and the gangue).

The main advantages of the interactive system application are:

- Replacing the old calculus method, where the subjectivism may introduce some errors in the calculus results;
- Offering the possibility to establish the optimum coals blend for the coal plant feeding, in correlation with the market demands and taking into account the washability and the coking properties of the rough coal;
- Allowing to use the selectivity indices of the concentration installations from practice in the efficiency indices;
- Assuring the data bases to elaborate and to assess a complex technical study depending on the concentrates quality, making up a scientific bases so useful for a profitable coal processing activity.

References

[1]. Popescu F., *Programarea și utilizarea calculatoarelor*, Editura Sigma Plus, Deva, 2002.
[2]. Popescu F., *Aplicații industriale ale tehnicii de calcul*, Editura AGIR, București, 2009.
[3]. Bădulescu C., *Procesarea diferitelor tipuri de deșeuri industrial*, Editura Universitas, Petrosani, 2021.
[4]. Bădulescu C., *Solubilization Processing of Ashes Power Plant*, Mining Revue, vol. 27, no. 1, p. 45-51, https://doi.org/10.2478/minrv-2021-0006, 2021.
[5]. Garaliu A., Ciocan V., Sârbu R., Zăvoianu C., *Implementarea unui nou sistem de apreciere a rezultatelor maximale posibil de realizat la uzinele de preparare a cărbunilor din Valea Jiului*, 7th BMPC, Vatra Dornei - România, p. 350-356, 28-30 mai 2007.
[6]. Krausz S., ***et al.***, *Study concerning the coal processing efficiency increasing for the processing plants in the Jiu Valley*, Petroșani, Petroșani, 1999.
[7]. Mihăilescu L., ***et al.***, *Modern Methods in the Coal Processing Efficiency Calculus*, Postgraudate coursebook, University of Petroșani, Romania.

THE ANNALS OF "DUNAREA DE JOS" UNIVERSITY OF GALATI
FASCICLE IX. METALLURGY AND MATERIALS SCIENCE
No. 2 - 2022, ISSN 2668-4748; e-ISSN 2668-4756
Article DOI: https://doi.org/10.35219/mms.2022.2.03

EFFECT OF THE FIBER ORIENTATION OF GLASS FIBER REINFORCED POLYMER COMPOSITES ON MECHANICAL PROPERTIES

Rodica CHIHAI (PEȚU), Claudia UNGUREANU, Vasile BRIA
"Dunarea de Jos" University of Galati, Research and Development Centre for Thermoset Matrix Composites, Cross-Border Faculty, Galati, Romania
e-mail: claudia.ungureanu@ugal.ro; vasile.bria@ugal.ro

ABSTRACT

Fiber reinforced polymer (FRP) composites possess excellent specific strength, specific stiffness and controlled anisotropy for which these are extensively used in various engineering applications, like automobile industries, aerospace industries, marine industries, space industries, electronics industries and many more. Glass fibers (GF), carbon fibers (CF) and aramid fibers (AF) are common reinforcements for polymer matrix composites (PMCs). High mechanical properties and wear resistance behaviour of glass fiber reinforced composites are the premises for the current experimental research on the effect of fiber orientation on the tensile strength of the polymeric composite materials. The glass fiber reinforced epoxy resin composite was prepared by wet lay-up method, followed by thermal treatment.

KEYWORDS: glass fiber, orientation, mechanical properties, epoxy resin

1. Introduction

Developing new composite materials from existing materials is the real challenge for most of the material engineers. So, there are huge research endeavours emerging in the field of composites to develop new materials with upgraded mechanical, electrical and thermal properties [1]. Among these composites, fiber reinforced polymer (FRP) offers not only high strength to weight ratio, but it also reveals exceptional properties like high strength, flexibility, stiffness and resistance to chemical harm. These wide ranges of diverse features have led composite materials to find significant applications in a variety of fields such as construction, mechanical, automobile, aerospace, and many other manufacturing industries [2, 3].

In order to get the best characteristics of the composites, different methods may be used, such as using hard materials like glass mats, silicone or ceramics, chemical additives or making coating layer [4]. Glass fiber (fiberglass) is one of the promising materials that can be used in laminate composite production. Fiberglass offers excellent strength and durability, thermal stability, resistance to impact, chemical, friction, and wear properties [5]. Also, it was demonstrated the increase of the tensile strength of the composite properties due to the fiber content [6, 7].

The arrangement and orientation of fibers define the properties and structural behavior of composite material [8, 9]. The fiber orientation mainly depends on the melt flow characteristics during manufacturing, which depend on rheological properties of the melt (viscosity, viscoelastic properties), processing parameters (injection temperature, pressure), product complex geometry (tool complexity) [10]. Literature also shows that fiber orientation significantly affects the mechanical properties of the SFRP. If fibers are longitudinally oriented (parallel to the loading direction), mechanical properties are improved due to the efficient load transfer from matrix to fiber, whereas in the case of transversely oriented fibers (perpendicular to the loading direction), only a small or negligible increase in mechanical properties is observed compared to the non-reinforced (or neat) material [11, 12]. Thus, the fiber orientation and distribution are parameters that are difficult to predetermine, yet it needs to be considered during product design and manufacturing.

As far as it is known, there are limited information on the application of oriented reinforced glass fiber as per its improved tensile properties.

THE ANNALS OF "DUNAREA DE JOS" UNIVERSITY OF GALATI
FASCICLE IX. METALLURGY AND MATERIALS SCIENCE
Nº. 2 - 2022, ISSN 2668-4748; e-ISSN 2668-4756
Article DOI: https://doi.org/10.35219/mms.2022.2.03

Because of the fact that it was determined that the polymer composites reinforced with fabrics and epoxy resins showed very good mechanical results during the research carried out over a long specific period of time [13-15], this paper aimed to analyse the behavior of the composite materials reinforced with glass fibers and homogeneous epoxy matrix.

2. Materials and methods

2.1. Materials

Epoxy resin has superior mechanical and electrical properties compared to other resins and it has good chemical and thermal resistance, but having high cross-linking, it sometimes suffers from brittleness and exhibits low impact properties, which can be improved by fabric reinforcement [16-20]. The experiments were carried out using the Epiphen system consisting of RE4020 (resin) and DE 4020 (hardener), with a 100:30 ratio [21, 22]. Generally, the producers give information regarding the natural polymerization at room temperature for 14 days, but to reach the best quality of the polymer, they also recommend thermal treatments. Glass fiber that has been used as reinforcement elements has a 280 g/m^2 specific weight and the thickness of 220 μm. This fiber has good reinforcement capability.

The samples used in this investigation were prepared using wet-lay-up technique and the concept of fiber orientation in the composite was equally adopted in this work in order to study the influence of the orientation of glass fiber on the tensile strength of the composite materials [23, 24]. The wet lay-up forming method is the most suitable when it is about forming particular fabric reinforced polymer composites, especially when the pot-time of the polymer is long enough to ensure a good penetration of the pre-polymer in-between the fiber threads.

It was formed of two composites made of 29 layers, which were denoted in this paper as M1 and M2. The M1 represents the materials where all the layers are orientated in the same direction and the layer configuration of the composite material M2 with the fabric orientation at various angles is presented in Table 1.

After the introduction of all layers, the mould was closed and placed in a horizontal position to ensure the quality of the structure and surfaces of the formed materials. For the formed materials, thermal treatment was applied (8 hours at 60 ºC, 2 hours at 80 ºC and 1 hour at 90 ºC) after the natural polymerization of polymer matrix of reinforced composites.

Table 1. *Orientation of the layers in the composite material*

No. layer	Orientation	No. layer	Orientation
1	0º	**16**	-30º
2	30º	**17**	0º
3	45º	**18**	30º
4	60º	**19**	45º
5	90º	**20**	60º
6	-60º	**21**	90º
7	-45º	**22**	-60º
8	-30º	**23**	-45º
9	0º	**24**	-30º
10	30º	**25**	0º
11	45º	**26**	30º
12	60º	**27**	45º
13	90º	**28**	60º
14	-60º	**29**	90º
15	-45º		

2.2. Tensile test

Tensile properties of the composites were performed according to ASTM D638-03. The tensile tests were done on Instron Universal Testing Machine with a maximum loading capacity of 100 kN. The tests were set for a loading speed of 5mm/minute and the stop condition was set at 50% drop of force or 50 mm displacement of grip. The standard tensile samples were extracted after the thermal treatment using a high-pressure water jet cutting machine. The specimen has the following dimensions: 57 mm in length X 13 mm of width X mm of thickness (Figure 1a).

THE ANNALS OF "DUNAREA DE JOS" UNIVERSITY OF GALATI
FASCICLE IX. METALLURGY AND MATERIALS SCIENCE
No. 2 - 2022, ISSN 2668-4748; e-ISSN 2668-4756
Article DOI: https://doi.org/10.35219/mms.2022.2.03

a b

Fig. 1. *a - The tensile test samples; b - Tensile test specimen holding in the Instron machine*

Figure 1b., shows the holding of a tensile test specimen on an *Instron* machine. For each composite panel, a set of five sample specimens were manufactured and tested. For post processing of the experimental results, a statistical analysis was performed based on the arithmetic mean with a negligible standard deviation.

3. Results and discussion

In the current study the composite material tensile strength was defined as the ultimate strength for which the total fracture of the known dog-bone specimen occurs.

Similar to other literature studies, as described by [25], the increase of the fiber content determined high mechanical properties as tensile, impact and flexural tendencies fiber on the reinforced polymer composites. As described by [26], the improving of the mechanical properties of fibre reinforced polymeric composites may be preferred to metal for some engineering applications.

In order to ensure the mechanical strength of the composite material in all directions, a special architecture was formed, namely the layers of fabrics in the formed composite were distributed at different angles fabric for the M2 material.

If we want to form a composite landmark, a landmark that presents a certain behavior in different directions, this behavior can be imprinted on the composite material from the design phase, by establishing the optimal architecture.

Figure 2-5 shows the tensile properties of the formed materials composite.

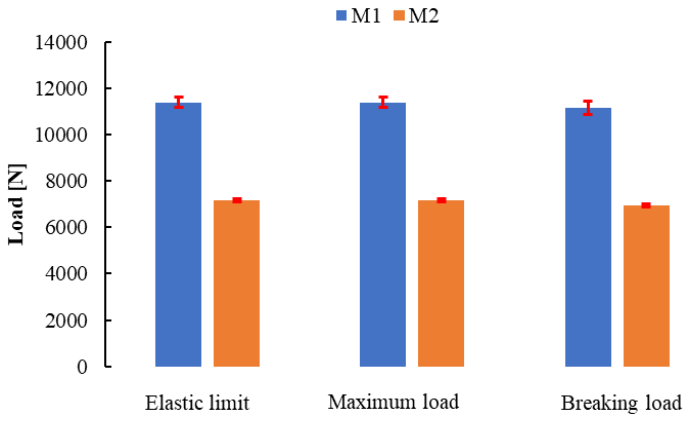

Fig. 2. *Maximum tensile load of formed materials*

THE ANNALS OF "DUNAREA DE JOS" UNIVERSITY OF GALATI
FASCICLE IX. METALLURGY AND MATERIALS SCIENCE
N°. 2 - 2022, ISSN 2668-4748; e-ISSN 2668-4756
Article DOI: https://doi.org/10.35219/mms.2022.2.03

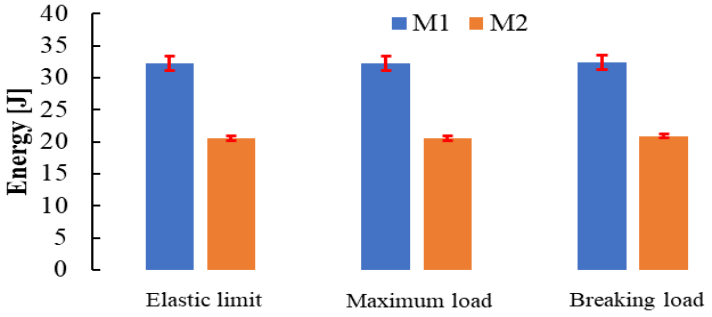

Fig. 3. *Energy to break of formed materials*

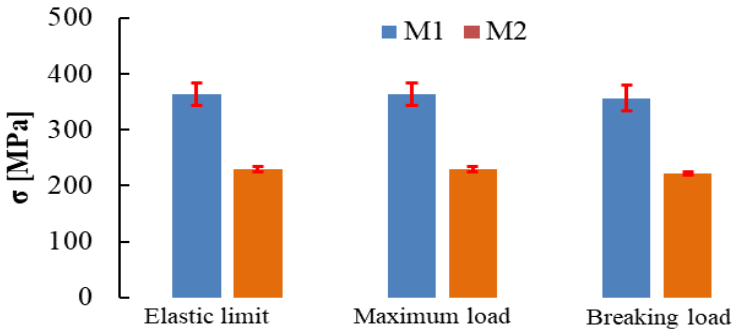

Fig. 4. *Tensile strength of formed materials*

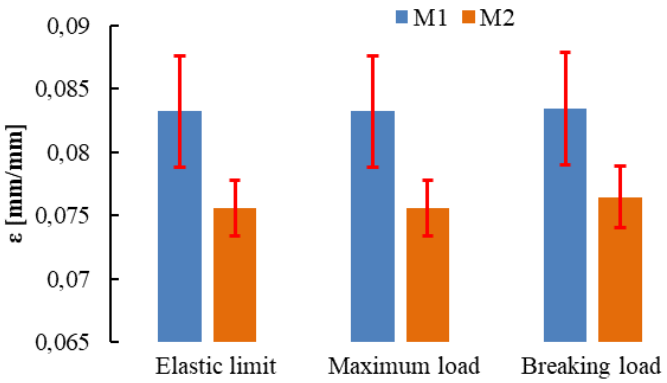

Fig. 5. *Tensile deformation*

From the error bars that represent the standard deviation, it denotes the fact that the values obtained from the 5 specimens are close. The difference between M1 and M2 can be explained by the ones described above, namely: only 28% of the fibers make the effort in the test direction.

From the graphs, it can be seen that M2 has a strength greater than 28% compared to M1, this indicates that the fibers oriented at 30°, 60° take on a full-length part of the force.

It can also be seen that the parameters shown on the graph for the 3 zones show approximately the same values, which indicates that the evolution of the force on the move is constant (linear). Therefore, the material exhibits identical mechanical behavior to tensile stresses.

Many studies have studied the effect of the reinforced glass fiber on the bulk mechanical properties of polymer composites [27-29]. It is widely acknowledged that the glass fiber, as the reinforced phase of the composites, bears more external load than the matrix does under the uniaxial tension. Specimens images after the test are shown in Figure 6.

THE ANNALS OF "DUNAREA DE JOS" UNIVERSITY OF GALATI
FASCICLE IX. METALLURGY AND MATERIALS SCIENCE
Nº. 2 - 2022, ISSN 2668-4748; e-ISSN 2668-4756
Article DOI: https://doi.org/10.35219/mms.2022.2.03

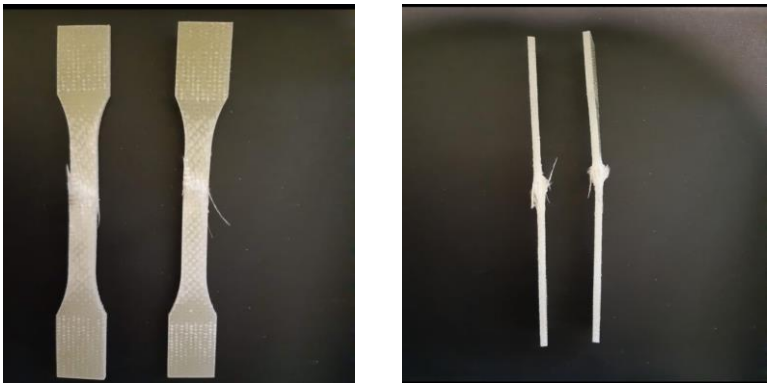

Fig. 6. *Specimens after the tensile test*

4. Conclusions

By subjecting a piece of fabric-reinforced composite material to physical stress, it is largely taken up by the fibers of the fabric. As the fibers in the fabric are oriented perpendicularly, it is obvious that the maximum strength of a fabric-reinforced composite landmark will be in both directions, warp and beat. If the composite material is formed by the overlapping of several equally oriented fabric starts, the maximum strength of the material will be in both directions.

In the case of material M2, the mechanical behavior is below the maximum values obtained, then in the case of material M1, it shows an approximately identical behavior in all directions, whereas material M1, although it has comparatively higher mechanical strength, this behavior is manifested only in both directions, beating and warping.

The parameter values in the case of material M1 are valid only in the 2 directions (0º, 90º), and on directions (30º, 60º, 45º) of the same material which has weak mechanical properties. However, this cannot be noticed in the case of the M2 material, which has significant amounts of fiber in those directions that can take over the tensile stress.

Acknowledgements

This research study was performed in the frame of Research and Development Center for Thermoset Matrix Composites (CCDCOMT).

References

[1]. Watt W., Perov B. V., *Handbook of Composites*, vol. 1, Strong Fibres, 1985.
[2]. Sherif G., Chukov D., Tcherdyntsev V., Torokhov V., *Effect of formation route on the mechanical properties of the polyethersulfone composites reinforced with glass fibers*, Polymers, 11 (8), 1364, 2019.
[3]. Vallittu P. K., Närhi T. O., Hupa L., *Fiber glass-bioactive glass composite for bone replacing and bone anchoring implants*, Dental Materials, 31 (4), p. 371-381, 2015.
[4]. Mohammed L., Ansari M. N., Pua G., Jawaid M., Islam M. S., *A review on natural fiber reinforced polymer composite and its applications*, International Journal of Polymer Science, 2015.
[5]. Neşer G., *Polymer based composites in marine use: history and future trends*, Procedia engineering, 194, p. 19-24, 2017.
[6]. Ahmad I., Baharum A., Abdullah I., *Effect of extrusion rate and fiber loading on mechanical properties of Twaron fiber-thermoplastic natural rubber (TPNR) composites*, Journal of reinforced plastics and composites, 25 (9), p. 957-965, 2006.
[7]. Zaini N. A. M., Ismail H., Rusli A., *Tensile, thermal, flammability and morphological properties of sepiolite filled ethylene propylene diene monomer (EDPM) rubber composites*, Iranian Polymer Journal, 27 (5), p. 287-296, 2018.
[8]. Agarwal B. D., Broutman L. J., Chandrashekhara K., *Analysis and performance of fiber composites*, John Wiley & Sons. Inc, New York, NY, 1990.
[9]. Ahivhare P. R., Bhalavi T., *Natural fibre reinforced polymer composite materials - A review*, Polym. Renew. Resource, 8, p. 71-78, 2017.
[10]. McNally D., *Short fiber orientation and its effects on the properties of thermoplastic composite materials*, 1977.
[11]. Nciri M., Notta-Cuvier D., Lauro F., Chaari F., Zouari B., Maalej Y., *A viscoelastic-viscoplastic model for short-fibre reinforced polymers with complex fibre orientations*, In EPJ Web of Conferences (vol. 94, p. 04008), EDP Sciences, 2015.
[12]. Notta-Cuvier D., Nciri M., Lauro F., Delille R., Chaari F., Robache F., Maalej Y., *Coupled influence of strain rate and heterogeneous fibre orientation on the mechanical behaviour of short-glass-fibre reinforced polypropylene*, Mechanics of Materials, 100, p. 186-197, 2016.
[13]. Wentzel D., Sevostianov I., *International Journal of Engineering Science*, 130, p. 129-135, https://doi. org/10.1016 /jijengsci.2018.05.012, 2018.
[14]. Forintos N., Czigány T., *Multifunctional application of carbon fiber reinforced polymer composites: Electrical properties of the reinforcing carbon fibers – A short review*, Composites Part B: Engineering, doi: 10.1016/j.compositesb.2018.10.098, 2018.
[15]. Peters S.-T., *Handbook of Composites*, 2, Ed. Green Gate Publishing Services, Tonbridge, England, p. 1-1052, ISBN 0-412-54020-7, 1998.
[16]. Ma R., Li W., Huang M., Feng M., Liu X., *The reinforcing effects of dendritic short carbon fibers for rigid polyurethane composites*, Composites Science and Technology, 170, p. 128-134, 2019.
[17]. Alam P., Mamalis D., Robert C., Floreani C., Brádaigh C. M. Ó., *The fatigue of carbon fibre reinforced plastics-A review*, Composites Part B: Engineering, 166, p. 555-579, 2019.
[18]. Morampudi P., Namala K. K., Gajjela Y. K., Barath M., Prudhvi G., *Review on glass fiber reinforced polymer composites*,

Materials Today: Proceedings, 43, p. 314-319, doi: 10.1016/j.matpr.2020.11.669, 2021.
[19]. Sahu N. P., Khande D. K., Patel G. C., Bohidar S. K., Sen P. K., *Study on aramid fibre and comparison with other composite materials*, International Journal for Innovative Research in Science & Technology, 1 (7), p. 303-306, 2014.
[20]. Vedrtnam A., *Novel method for improving fatigue behavior of carbon fiber reinforced epoxy composite*, Composites Part B: Engineering, 157, p. 305-321, 2019.
[21]. ***, http://www.polydis.ro/wp-content/uploads/2014/08/Epiphen-4020.pdf.
[22]. Jin F.-L., Li X., Park S.-J., *Synthesis and application of epoxy resins: A review*, Journal of Industrial and Engineering Chemistry, 29, 1-11, doi: 10.1016/j.jiec.2015.03.026, 2015.
[23]. Shekar K. C., Singaravel B., Prasad S. D., Venkateshwarlu N., *Effect of Fiber Orientation on the Flexural Properties of Glass Fiber Reinforced*, Epoxy- Matrix Composite, Materials Science Forum, 969, p. 502-507, doi: 10.4028/www.scientific.net/msf.969.502, 2019.
[24]. Prasanth S. I., Kesavan K., Kiran P., Sivaguru M., Sudharsan R., Vijayanandh R., *Advanced structural analysis on e-glass fiber reinforced with polymer for enhancing the mechanical properties by optimizing the orientation of fiber*, Proceedings of advanced material, Engineering & Technology, doi: 10.1063/5.0019378, 2020.
[25]. Chen R. S., Muhammad Y. H., Ahmad S., *Physical, mechanical and environmental stress cracking characteristics of epoxy/glass fiber composites: Effect of matrix/fiber modification and fiber loading*, Polymer Testing, 96, 107088, 2021.
[26]. Bahl S., *Fiber reinforced metal matrix composites - a review*, Materials Today: Proceedings, doi: 10.1016/j.matpr.2020.07.423, 2020.
[27]. Xian G., Guo R., Li C., *Combined effects of sustained bending loading, water immersion and fiber hybrid mode on the mechanical properties of carbon/glass fiber reinforced polymer composite*, Composite Structures, 281, 115060, 2022.
[28]. Babazadeh J., Rahmani K., Hashemi S. J., Sadooghi A., *Effect of glass, carbon, and kevlar fibers on mechanical properties for polymeric composite tubes produced by a unidirectional winding method*, Materials Research Express, 8 (4), 045301, 2021.
[29]. Wang C., Zhang Y., Yi Y., Lai D., Yang J., Wang W., *Thermal, morphological and mechanical properties of glass fiber reinforced star-branched polyamide 6*, Polymer Composites, 2022.

THE ANNALS OF "DUNAREA DE JOS" UNIVERSITY OF GALATI
FASCICLE IX. METALLURGY AND MATERIALS SCIENCE
Nº. 2 - 2022, ISSN 2668-4748; e-ISSN 2668-4756
Article DOI: https://doi.org/10.35219/mms.2022.2.04

MATLAB PROGRAM FOR DETERMINING THE INERTIA CHARACTERISTICS OF FLAT SURFACES WITH MONTE CARLO ALGORITHMS

Marius BOTIȘ, Costel PLEȘCAN*
Transilvania University of Brașov, Department of Civil Engineering, Romania
e-mail: *plescan.costel@unitbv.ro

ABSTRACT

This paper presents a Matlab program for calculating the inertia tensor for complex plane surfaces. The calculation of the moments of inertia for plane surfaces with classical methods involves decomposing the surfaces into primitive surfaces and applying Steiner's relations. The classical methods are based on the knowledge of the analytical determined moments of inertia for primitive surfaces. In the case of complex surfaces, numerical methods can be used which are based on discretizing the surface into triangles and determining the moments of inertia by applying Steiner's relations knowing the analytical moments of inertia for a triangle. Both methods are computationally intensive and are basically based on the analytical moments of inertia of an elementary surface. In the case of large and complex surfaces the Monte Carlo algorithm can be used, which is a probabilistic algorithm based on the generation of area elements within the surface for which the moments of inertia are determined and then summed over the entire area bounded by the surface. The paper presents the Matlab calculation program and application examples for the use of the probabilistic Monte Carlo algorithm.

KEYWORDS: Monte Carlo method, moments of inertia of flat surfaces, probabilistic algorithms

1. Introduction

In order to determine how to calculate moments of inertia for plane surfaces with the Monte Carlo method, we will start with the calculation of moments of inertia of a concentrated mass system. If we consider n concentrated masses into which a surface decomposes, then the moments of inertia [1] of that surface with respect to the x and y axes of a coordinate system attached to the surface are:

Axial moments of inertia:

$$J_{xx} = \int_A y^2 dm = \sum_{i=1}^{n} m_i y_i^2 . \quad (1)$$

$$J_{yy} = \int_A x^2 dm = \sum_{i=1}^{n} m_i x_i^2 \quad (2)$$

Centrifugal moment of inertia:

$$J_{xy} = \int_A xy dm = \sum_{i=1}^{n} m_i x_i y_i \quad (3)$$

Polar moment of inertia:

$$J_p = \sum_{i=1}^{n} m_i y_i^2 + \sum_{i=1}^{n} m_i x_i^2 \quad (4)$$

The tensor of mechanical moments of inertia in matrix form becomes:

$$[J] = \begin{bmatrix} J_{xx} & J_{xy} \\ J_{yx} & J_{yy} \end{bmatrix} = \begin{bmatrix} \sum_{i=1}^{n} m_i y_i^2 & -\sum_{i=1}^{n} m_i x_i y_i \\ -\sum_{i=1}^{n} m_i x_i y_i & \sum_{i=1}^{n} m_i x_i^2 \end{bmatrix} \quad (5)$$

Similarly, the tensor of geometric moments of inertia becomes:

THE ANNALS OF "DUNAREA DE JOS" UNIVERSITY OF GALATI
FASCICLE IX. METALLURGY AND MATERIALS SCIENCE
No. 2 - 2022, ISSN 2668-4748; e-ISSN 2668-4756
Article DOI: https://doi.org/10.35219/mms.2022.2.04

$$[J] = \begin{bmatrix} \sum_{i=1}^{n} m_i y_i^2 & -\sum_{i=1}^{n} m_i x_i y_i \\ -\sum_{i=1}^{n} m_i x_i y_i & \sum_{i=1}^{n} m_i x_i^2 \end{bmatrix} = \rho t \begin{bmatrix} \sum_{i=1}^{n} A_i y_i^2 & -\sum_{i=1}^{n} A_i x_i y_i \\ -\sum_{i=1}^{n} A_i x_i y_i & \sum_{i=1}^{n} A_i x_i^2 \end{bmatrix} \quad (6)$$

In relation (7) the connection between the tensor of geometrical moments of inertia and the tensor of the mechanical moments of inertia is presented.

$$[J] = \rho t [I] \quad (7)$$

where:

- ρ is the material density of the surface;
- t is the thickness of the surface.

From relations (6) and (7) it can be noted that knowing the geometric inertia tensor of the surface allows the determination of the mechanical inertia tensor if the thickness and material density of the surface are known.

2. The algorithm for calculating the inertia tensor with the Monte Carlo method

To determine the inertia tensor with the Monte Carlo method for plane surfaces, the surface is decomposed into a system of concentrated masses for which the moments of inertia can be determined with relations (1)-(4). The mass elements dm are obtained by dividing the surface mass M by the number of probabilistically generated elements N according to relation (8).

$$dm = \frac{M}{N} \quad (8)$$

N is the number of probabilistically generated points in the surface domain for which the moments of inertia are determined; -M the total mass of the surface. The higher the number of points generated on the surface domain, the higher the probability of tending to the exact solution. Using the Monte Carlo algorithm, one can determine both the geometric and the mechanical inertia tensor with the relationships shown below. Mechanical moment of inertia tensor:

$$[J] = \begin{bmatrix} J_{xx} & J_{xy} \\ J_{yx} & J_{yy} \end{bmatrix} = \begin{bmatrix} \sum_{i=1}^{N} dm y_i^2 & -\sum_{i=1}^{N} dm x_i y_i \\ -\sum_{i=1}^{N} dm x_i y_i & \sum_{i=1}^{N} dm x_i^2 \end{bmatrix}; dm = \frac{M}{N}; (x_i\ y_i) \epsilon A \quad (9)$$

Tensor of geometric moments of inertia:

$$[I] = \begin{bmatrix} I_{xx} & I_{xy} \\ I_{yx} & I_{yy} \end{bmatrix} = \begin{bmatrix} \sum_{i=1}^{N} dA y_i^2 & -\sum_{i=1}^{N} dA y_i \\ -\sum_{i=1}^{N} dA x_i y_i & \sum_{i=1}^{N} dA x_i^2 \end{bmatrix}; dA = \frac{A}{N}; (x_i\ y_i) \epsilon A \quad (10)$$

where:

- A is the area of the surface;
- x_i, y_i are the coordinates of the concentrated masses dm.

3. Presentation of Matlab programs for the calculation of the inertia tensor on plane surfaces with the probabilistic Monte Carlo method

In order to validate the probabilistic Monte Carlo algorithm for the calculation of the inertia tensor in the case of flat surfaces, the implementation of the algorithm in Matlab code is presented below. The inertia tensor is calculated for a square and a triangle. In both cases the moments of inertia are determined analytically and probabilistically for comparison.

3.1. The implementation of the Monte Carlo algorithm in MATLAB program in the case of a square

Matlab code implementation of the Monte Carlo method [2] for determining the moments of inertia for a square of mass M, the axial moments of inertia and the centrifugal moment of inertia for a square have the analytical expressions below:

Axial moments of inertia:

$$I_{yy} = I_{xx} = \frac{1}{3} M a^2 \quad (11)$$

THE ANNALS OF "DUNAREA DE JOS" UNIVERSITY OF GALATI
FASCICLE IX. METALLURGY AND MATERIALS SCIENCE
No. 2 - 2022, ISSN 2668-4748; e-ISSN 2668-4756
Article DOI: https://doi.org/10.35219/mms.2022.2.04

Centrifugal moment of inertia:

$$I_{xy} = -\frac{1}{4}Ma^2 \quad (12)$$

The Matlab program [3] for determining the inertial characteristics for the square with the probabilistic Monte Carlo method is presented below:

```
clear;
%Calculation of moments of inertia for a square
M=1;% mass of square
a=1;% the square side where infinitesimal masses are randomly generated
N=3000;%number of infinitesimal masses
dm=M/N;% infinitesimal mass element
Ixx=0;
Iyy=0;
Ixy=0;
n=0;%initializations
while n<N
x=a*rand;
y=a*rand;
scatter(x,y,40,'MarkerEdgeColor',[0 0 0],...
        'MarkerFaceColor',[1 0 0],...
        'LineWidth',2)
hold on;
rtemp=[x y];
%Theoretical values of moment of inertia
Ixx=Ixx+dm*(y^2);
Iyy=Iyy+dm*(x^2);
Ixy=Ixy-dm*(x*y);
n=n+1;
end
hold off;
Ixxt=1/3*M*a^2;
Iyyt=1/3*M*a^2;
Ixyt=-M*a^2/4;
disp('Theoretical value of moment of inertia Ixxt =');
disp(Ixxt);
disp('Value moment of inertia with Monte Carlo Ixx=');
disp(Ixx);
disp('Theoretical value of moment of inertia Iyyt =');
disp(Iyyt);
disp('Value moment of inertia with Monte Carlo Iyy=');
disp(Iyy);
disp('Theoretical value of moment of inertia Ixyt =');
```

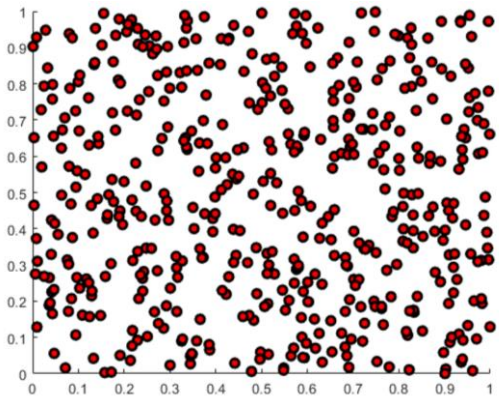

Fig. 1. *Generating 500 points randomly*

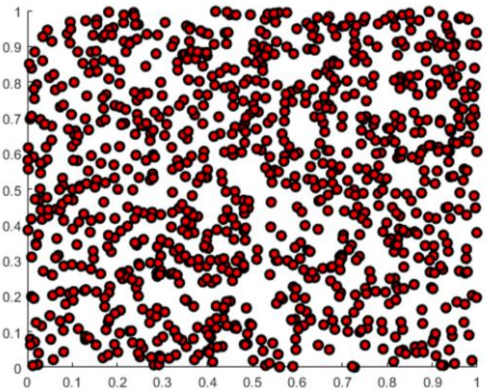

Fig. 2. *Generating 1000 points randomly*

Following the analysis, the results presented in Fig. 1 and Fig. 2 were obtained, which are compared with the analytical results obtained.

For 500 randomly generated points Fig. 1, the theoretical and probabilistic results are:

Theoretical value of moment of inertia Ixxt = 0.3333

Value moment of inertia with Monte Carlo Ixx = 0.3233

Theoretical value of moment of inertia Iyyt = 0.3333

Value moment of inertia with Monte Carlo Iyy = 0.3466

Theoretical value of the moment of inertia Ixyt = -0.2500

Value moment of inertia with Monte Carlo Ixy = -0.2480

For 1000 randomly generated points Fig. 2, the theoretical and probabilistic results are

Theoretical value of moment of inertia Ixxt = 0.3333

Value moment of inertia with Monte Carlo Ixx = 0.3283

Theoretical value of moment of inertia Iyyt = 0.3333

THE ANNALS OF "DUNAREA DE JOS" UNIVERSITY OF GALATI
FASCICLE IX. METALLURGY AND MATERIALS SCIENCE
No. 2 - 2022, ISSN 2668-4748; e-ISSN 2668-4756
Article DOI: https://doi.org/10.35219/mms.2022.2.04

Value moment of inertia with Monte Carlo Iyy = 0.3247

Theoretical value of the moment of inertia Ixyt = -0.2500

Value moment of inertia with Monte Carlo Ixy = -0.2407

3.2. Implementation of Monte Carlo algorithm in MATLAB program in the case of a triangle

In the following, it is presented the MATLAB implementation of the Monte Carlo method [2] for determining the moments of inertia for an isosceles triangle of mass M. The axial moments of inertia and the centrifugal moment of inertia have the analytical expressions below:

Axial moments of inertia:

$$I_{yy} = I_{xx} = \frac{1}{6}Ma^2 \tag{13}$$

Centrifugal moment of inertia:

$$I_{xy} = -\frac{1}{12}Ma^2 \tag{14}$$

The Matlab program [3] for determining the inertial characteristics for the triangle with the probabilistic Monte Carlo method is presented below:

```
clear;
%Calculation of moments of inertia for a triangle
M=1;% mass of triangle
a=1;% the square side where infinitesimal masses are randomly generated
N=1000;%number of infinitesimal masses
dm=M/N;% infinitesimal mass element
Ixx=0;Iyy=0;Ixy=0;n=0;%initializations
while n<N
x=a*rand;y=a*rand;
rtemp=[x y ];
if (rtemp(:,1)+rtemp(:,2)<1)
scatter(x,y,40,'MarkerEdgeColor',[0 0 0],...
        'MarkerFaceColor',[1 0 0],...
        'LineWidth',2)
hold on;
Ixx=Ixx+dm*(y^2);Iyy=Iyy+dm*(x^2);Ixy=Ixy-dm*(x*y);
n=n+1;
end
end
hold off;
Ixxt=1/6*M*a^2;Iyyt=1/6*M*a^2;Ixyt=-M*a^2/12;
disp('Theoretical value of moment of inertia Ixxt =');
disp(Ixxt);
disp('Value moment of inertia with Monte Carlo Ixx=');
disp(Ixx);
disp('Theoretical value of moment of inertia Iyyt =');
disp(Iyyt);
disp('Value moment of inertia with Monte Carlo Iyy=');
disp(Iyy);
disp('Theoretical value of moment of inertia Ixyt =');
disp(Ixyt);
disp('Value moment of inertia with Monte Carlo Ixy=');
disp(Ixy);
```

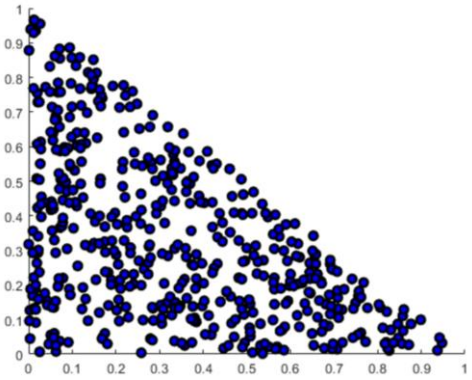

Fig. 3. *Generating 500 points randomly*

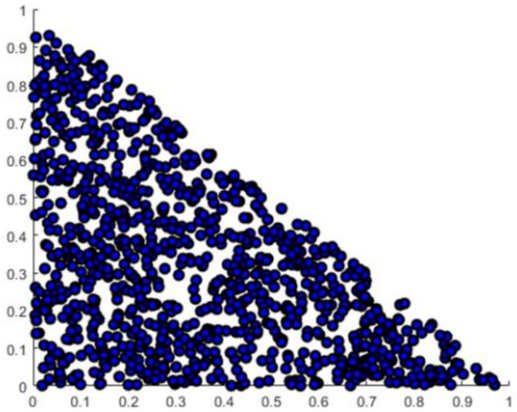

Fig. 4. *Generating 500 points randomly*

For 500 randomly generated points in Fig. 3, the theoretical and probabilistic results are:

Theoretical value of moment of inertia Ixxt = 0.1667

Value moment of inertia with Monte Carlo Ixx = 0.1635

THE ANNALS OF "DUNAREA DE JOS" UNIVERSITY OF GALATI
FASCICLE IX. METALLURGY AND MATERIALS SCIENCE
Nº. 2 - 2022, ISSN 2668-4748; e-ISSN 2668-4756
Article DOI: https://doi.org/10.35219/mms.2022.2.04

Theoretical value of moment of inertia Iyyt = 0.1667

value moment of inertia with Monte Carlo Iyy = 0.1745

Theoretical value of moment of inertia Ixyt = -0.0833

Value moment of inertia with Monte Carlo Ixy = -0.0812

For 1000 randomly generated points Fig. 4, the theoretical and probabilistic results are:

Theoretical value of moment of inertia Ixxt = 0.1667

Value moment of inertia with Monte Carlo Ixx = 0.1619

Theoretical value of moment of inertia Iyyt = 0.1667

value moment of inertia with Monte Carlo Iyy = 0.1619

Theoretical value of moment of inertia Ixyt = -0.0833

Value moment of inertia with Monte Carlo Ixy = -0.0813

4. Results and conclusions

The results of the analysis showed:

- The Monte Carlo algorithm has a probabilistic character due to the random generation of elementary dm masses;
- The results obtained depend on the number of dm masses in the surface domain for which the inertia tensor is determined;
- The presented method can be applied in the case of large and complex surfaces where classical analytical methods or numerical methods require a very large volume of calculations.
- Results obtained with Matlab [3] have been validated for square and triangle surfaces.

References

[1]. Billingsley J., *Essentials of Dynamics and Vibration*, In: Publishing House Springer, 2018.
[2]. Barbu A., Zhu S., *Monte Carlo Methods*, In: Publishing House Springer, 2020.
[3]. ***, https://www.mathworks.com/products/matlab.html, Accessed: 22.00.2021.

THE ANNALS OF "DUNAREA DE JOS" UNIVERSITY OF GALATI
FASCICLE IX. METALLURGY AND MATERIALS SCIENCE
Nº. 2 - 2022, ISSN 2668-4748; e-ISSN 2668-4756
Article DOI: https://doi.org/10.35219/mms.2022.2.05

STUDIES AND RESEARCH ON ELECTROCHEMICALLY OBTAINING ZINC MATRIX COMPOSITE MATERIALS USING THE Al_2O_3 DISPERSION PHASE

Simona BOICIUC
"Dunarea de Jos" University of Galati, Romania
e-mail: simona_boiciuc@yahoo.com

ABSTRACT

The paper presents the electrochemical production of composite zinc matrix coatings using Al_2O_3 as dispersed phases. It was found that by correlating the working parameters with the concentration of the dispersed phase in the electrolyte, the mechanical characteristics and the corrosion resistance of the deposits could be improved.

KEYWORDS: Zn composite coatings, electrodeposition, Al_2O_3, corrosion in saline fog

1. Introduction

Electrochemical galvanizing was initially applied to improve the corrosion resistance of ferrous materials (steels, cast iron). Following the improvement of the processes of further treatment of zinc deposits by bleaching (nitrogen neutralization), passivation, staining, coatings were included in the category of protector – decorative. In order to improve the mechanical properties of coatings, respectively to decrease internal stresses and fragilization and to increase ductility, coatings may be subject to dehydrogenation [1].

The behavior of zinc-based deposits is influenced by the climatic conditions of exploitation. They are heavily attacked in an industrial atmosphere containing sulphur dioxide, and on their surface water-soluble corrosion products were formed. In conditions of indoor atmosphere and moderate humidity these coatings have a high stability. They are resistant to corrosion by various lubricants and solvents, including chlorinated ones, of water, except for the marine ones.

Zinc-based coatings are stable in dry air, but in humid air and water with carbon dioxide, oxygen, sulphates, they are covered with carbonate, oxide, sulfate films that protect the metal against corrosion.

The thickness of the layers deposited must take into account the degree of aggressiveness of the environment, being thicker the more difficult the operating conditions are.

In addition, the zinc coating on steel in the atmosphere at normal temperature is anodic (due to the pronounced electronegative character of zinc), but, by heating over 70 ºC it becomes cathodic [2].

Thus, the existence of discontinuities such as pores, cracks, exfoliations in the deposited layer leads to the formation of local galvanic elements that can influence the behavior in case of corrosion. The metal in the deposited layer, since it is more electronegative, becomes anode and corrodes, and the support (the metal of the piece) becomes cathode, thus being protected. However, over time, the appearance of deposits changes due to the coating with corrosion products [3].

Due to the anterior mentioned properties and the low-cost price, zinc-based coatings are applied for the corrosion protection of parts in the car building industry, electronics and electrotechnics industry, petroleum, consumer goods.

The use of alumina as a dispersed phase in the production of composite coatings is due to its mechanical and chemical characteristics: it is hard (hardness 9 on the Mohs scale), chemically inert (it does not dissolve in water or in mineral acids, being attacked only by alkaline hydroxides and bi-sulphates in the melt and by phosphoric acid) and has the ability to take various forms and perform various functions [4, 5].

The research carried out aims to obtain composite coatings with zinc base by electrochemical means using technical alumina particles (contains 98.5% γ - Al_2O_3 and maximum 10% - α - Al_2O_3) as dispersed phase, with dimensions of approx. 5 µm and their characterization.

THE ANNALS OF "DUNAREA DE JOS" UNIVERSITY OF GALATI
FASCICLE IX. METALLURGY AND MATERIALS SCIENCE
No. 2 - 2022, ISSN 2668-4748; e-ISSN 2668-4756
Article DOI: https://doi.org/10.35219/mms.2022.2.05

2. Experimental conditions

The quality of the coating depends on the surface roughness and the working parameters: the composition of the electrolyte, the current density, the temperature of the electrolyte bath, the agitation of the solution, the pH, the movement of the electrodes.

The electrolyte used in the experimental research consisted of: $ZnSO_4$ x $7H_2O$ – 310 g/L, Na_2SO_4 x $10H_2O$ – 75 g/L, $Al_2(SO_4)_3$ x $18H_2O$ – 30 g/L, pH = 3.8-4.4.

The current density used for deposits was 3 A/dm^2, the rotation speed 1000 rpm, the deposition time 60 minutes. Alumina was used as a dispersed phase at a concentration of 10-30 g/L.

High purity zinc (99.99%) was used as an anode, and the cathode (support material) was made of steel tape (0.1 %C).

The use of $Na2SO_4$ x $10H_2O$ was done in order to increase the electrical conductivity, dispersion capacity and to decrease the electrolysis voltage.

The use of $Al_2(SO_4)_3$ x $18H_2O$ was done in order to stabilize the acidity of the electrolyte as a result of the increase in cathodic overvoltage. Deposits with lower roughness can thus be obtained.

Before submitting the samples, they have undergone preparatory operations as follows:

- Pre-degreasing - it was carried out in a mixture of benzene and acetone for the removal from the surface of the sheet of fat soluble in organic solvents; the immersion time was 5-10 minutes, and the working temperature was approx. 18-25 ^oC;

- Chemical degreasing - for the removal of unsaponifiable fats; the solution used consists of: sodium hydroxide 20 g/L, sodium carbonate 45 g/L, trisodium phosphate 20 g/L, surfactant 3 g/L; the working temperature was 70-75 ^oC, degreasing time 20-30 seconds; after degreasing the samples were washed with demineralized water at a temperature of 60-65 ^oC for 3-5 minutes;

- Pickling - was carried out in 20% hydrochloric acid solution, at a temperature of 18-25 ^oC, for 1-2 minutes; after pickling the samples were washed intensively with cold water for 3-5 minutes.

The thicknesses of the obtained layers were determined with a Phynix Pocket Surfix device, and the roughnesses with a Namicon TR 100 device.

The micro-hardenings of the layers obtained were determined using a PMT3 microdurmeter with a load of 50 g.

The obtained layers were subjected to salt mist corrosion, in accordance with ISO 9227/2012, for a period of 96 hours.

To carry out the diffractometric analysis, the diffractometer DRON 3 with copper anticatode, monochromatized diffracted beam, U = 34 kV, I = 30 mA; F1 = 2 mm; F2 = 0.5 mm; ω = 1°/min; vband = 720 mm/h, at the variation of the diffraction angle within the limits 2θ = 20°....75°.

3. Experimental results

The powder used in the experimental research was analysed through X-ray diffraction.

The results obtained from the diffractometric analysis are presented in Table 1 and the corresponding diffractogram in Figure 1.

Analysing Table 1 and Figure 1, it can be seen that the two forms α and γ of the technical alumina have been identified.

Pure zinc deposits were made and with different phase concentrations dispersed in the electrolyte, respectively sample P1-10 g/L, P2-20 g/L, P3-30 g/L of alumina.

Table 1. *Diffractometric analysis of alumina powder*

Phase identified	Diffraction angle Bragg 2θ [°]	Muller indices (hkl)	Interplanar distance d/n [A]
Al_2O_3 - α	41.09	(112)	2.55
Al_2O_3 - α	44.38	(101)	2.37
Al_2O_3 - α	50.97	(102)	2.08
Al_2O_3 - γ	55.75	(200)	1.98
Al_2O_3 - γ	60.90	(222)	1.763
Al_2O_3 - α	61.95	(202)	1.74
Al_2O_3 - α	68.52	(123)	1.59
Al_2O_3 - α	71.07	(212)	1.54
Al_2O_3 - α	72.27	(233)	1.50
Al_2O_3 - γ	79.48	(220)	1.40
Al_2O_3 - α	81.59	(112)	1.37
Al_2O_3 - α	23.09	(234)	1.23

THE ANNALS OF "DUNAREA DE JOS" UNIVERSITY OF GALATI
FASCICLE IX. METALLURGY AND MATERIALS SCIENCE
No. 2 - 2022, ISSN 2668-4748; e-ISSN 2668-4756
Article DOI: https://doi.org/10.35219/mms.2022.2.05

By analysing Fig. 2, it can be found that when increasing the concentration of the dispersed phase in the electrolyte, the thickness of the deposited layer increases from 62.5 µm for the pure zinc sample to 69 µm for the sample with a concentration of the dispersed phase of 30 g/L.

Following the determination of the roughness of the deposited layers, Fig. 3, it was found that it decreased compared to the deposition of pure zinc. The presence of dispersed phase particles changes the mechanism of growth of crystals, favouring nucleation, which leads to the finishing of the structure, thus decreasing the roughness of deposits. However, when the concentration of the dispersed phase in the electrolyte is increased, the roughness is increased. The roughness of the support was 0.633 µm resulting from processing with abrasive material.

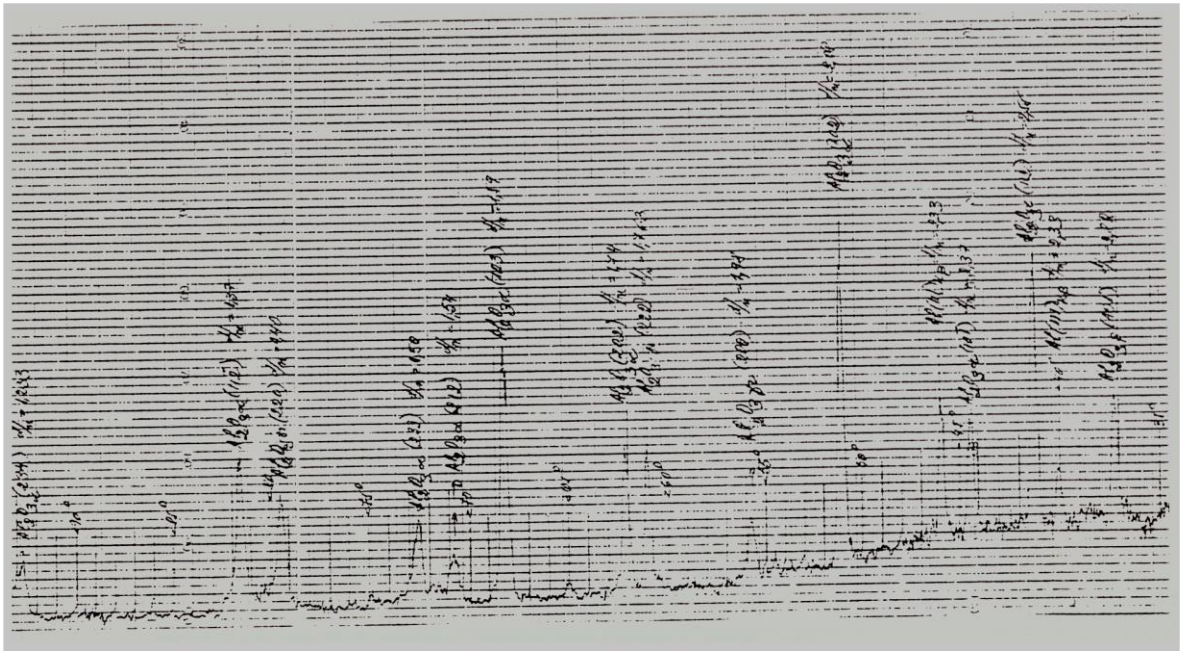

Fig. 1. *Alumina powder diffractogram* [6]

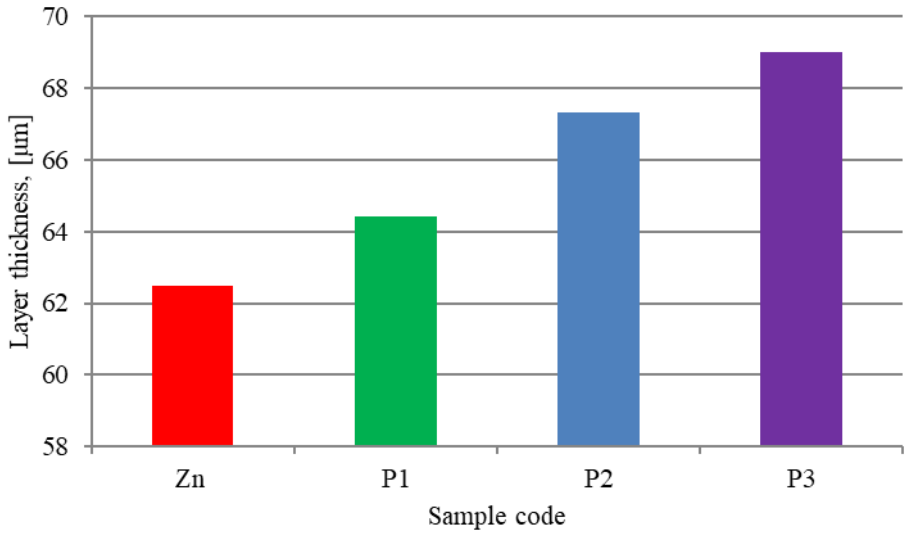

Fig. 2. *Variation of the thickness of the deposited layers with the dispersed phase concentration*

THE ANNALS OF "DUNAREA DE JOS" UNIVERSITY OF GALATI
FASCICLE IX. METALLURGY AND MATERIALS SCIENCE
No. 2 - 2022, ISSN 2668-4748; e-ISSN 2668-4756
Article DOI: https://doi.org/10.35219/mms.2022.2.05

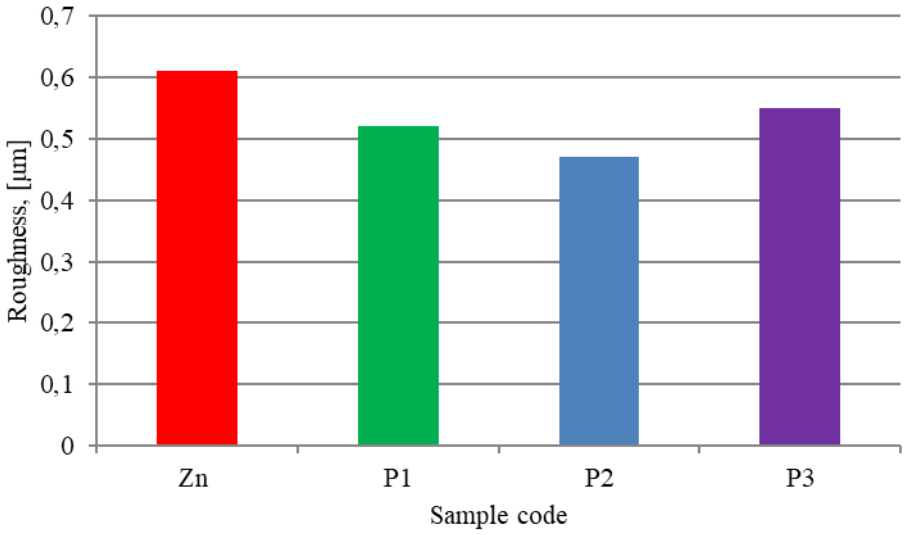

Fig. 3. *Variation of roughness of deposits with dispersed phase concentration*

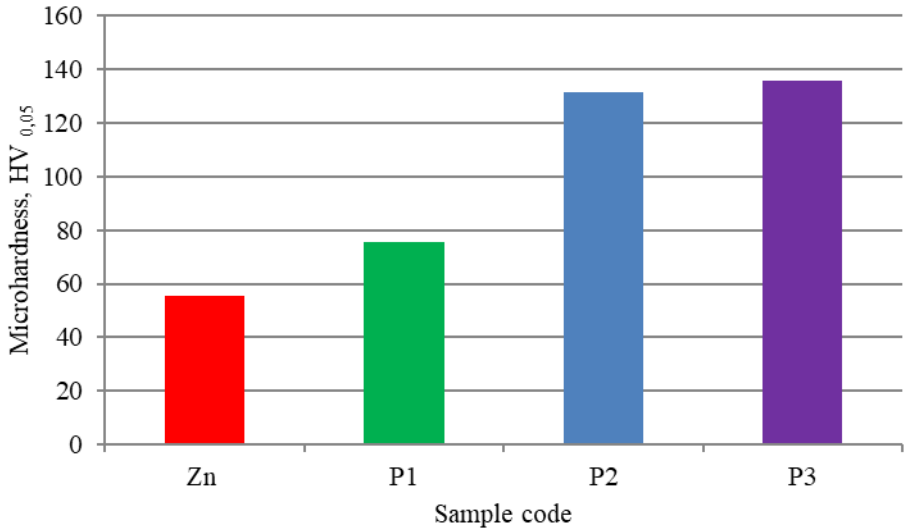

Fig. 4. *Variation of hardness of deposits with dispersed phase concentration in electrolyte*

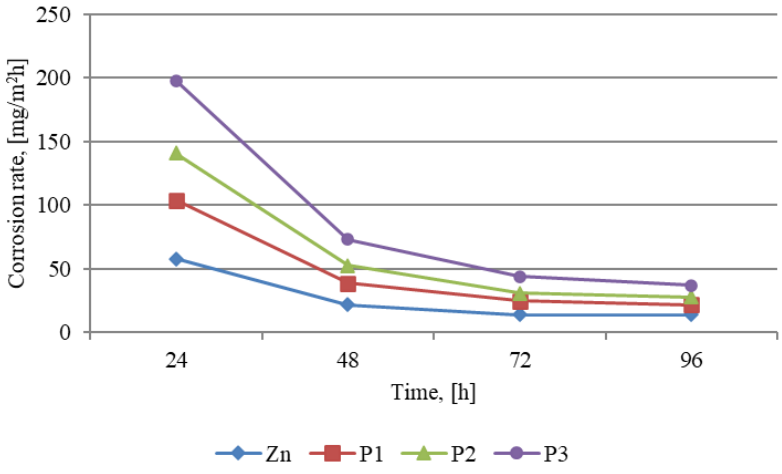

Fig. 5. *Corrosion behavior in salt mist of obtained coatings*

THE ANNALS OF "DUNAREA DE JOS" UNIVERSITY OF GALATI
FASCICLE IX. METALLURGY AND MATERIALS SCIENCE
No. 2 - 2022, ISSN 2668-4748; e-ISSN 2668-4756
Article DOI: https://doi.org/10.35219/mms.2022.2.05

The salt fog corrosion behavior of the deposited layers, Fig. 5, revealed a superior resistance of composite coatings compared to the deposition of pure zinc. The best behavior was presented by sample P2 with 20 g/L dispersed phase. Thus, if for the same current density, the concentration of the dispersed phase in the electrolyte increases, the roughness increases, which favours the corrosion processes. There is a corrosion at points which evolve during the said period, depending on the passivation of the surface.

Corrosion is favoured by the presence of pore-like defects, bathroom inclusions or microcracks caused by the local increase of internal stresses. Corrosion can spread around defects, and by accumulating corrosion products in them, exfoliation of the layer can occur.

4. Conclusions

Following the experimental researches carried out, the following conclusions can be mentioned:

- Composite coatings with zinc matrix and alumina dispersed phase exhibit superior properties to pure zinc deposits. It gives hardness and thus resistance to continuous wear, resistance to corrosion, ensures a pleasant, decorative look and extends the service life of parts.

- Unlike the zinc layers obtained through other processes, those electrochemically made have more uniform thicknesses, influenced by the parameters of deposition. It was found that increasing the concentration of the dispersed phase in the electrolyte, it increased the thickness of the deposited layer from 62.5 µm for the pure zinc sample to 69 µm for the composite coating with 30 g/L dispersed phase.

- When increasing the dispersed phase concentration in the electrolyte, the roughness of the coatings was increased from 0.52 µm for 10 g/L to 0.55 µm for 30 g/L. Compared to the deposition of pure zinc (roughness 0.61 µm), there is a decrease in the size of the crystallites, which causes a decrease in the roughness.

- The composite coatings obtained have higher hardness compared to the deposition of pure zinc (55.7 daN/mm^2). They range from 75.6 daN/mm^2 for a dispersed phase concentration of 10 g/L to 135.7 daN/mm^2 for a dispersed phase concentration of 30 g/L. Hardening is due to the dispersion of alumina particles in the zinc matrix, the finishing of the grain and the increase of the deformation resistance (due to the change in the displacement of structural defects).

- Composite coatings exhibit better corrosion behavior in saline fog compared to the deposition of pure zinc. With the increase of the dispersed phase concentration in the electrolyte, due to the increase of roughness, the corrosion rate increases.

References

[1]. Marinescu A., Andonianț Gh., **Bay E.**, *Tehnologii electrochimice şi chimice de protectie a materialelor metalice*, Editura Tehnica, Bucureşti, 1984.

[2]. Maria Constantinescu, *Protecţia anticorozivă a metalelor*, Editura Tehnică, Bucureşti, 1979.

[3]. Vermeşan G., *et al.*, *Introducere în ingineria suprafeţelor*, Editura Dacia, Cluj-Napoca, 1999.

[4]. Muşat V., *Ceramică avansată*, Editura tehnică, Bucureşti, 2001.

[5]. Constantinescu I., Oprea F., Mitoseriu O., *A comparative study of the properties of Zinc-SiO_2 and Zinc-Al_2O_3 composite layers*, The 4th International Conference "Advanced Composite Materials Engineering", COMAT 2012, Brasov, Romania, 18-20 October 2012.

[6]. Boiciuc S., *Studies and research on the influence of deposit parameters on the characteristics of composite coatings Ni – Al_2O_3 obtained by electrochemical methods*, The Annals of "Dunarea de Jos" University of Galati Fascicle IX. Metallurgy and Materials Science, No. 3, p. 17-21, ISSN 2668-4748; e-ISSN 2668-4756, 2021.

THE ANNALS OF "DUNAREA DE JOS" UNIVERSITY OF GALATI
FASCICLE IX. METALLURGY AND MATERIALS SCIENCE
N°. 2 - 2022, ISSN 2668-4748; e-ISSN 2668-4756
Article DOI: https://doi.org/10.35219/mms.2022.2.06

OBTAINING THIN FILMS OF ZnO THROUGH THERMAL EVAPORATION IN VACUUM AND OXIDATION

Simona BOICIUC
"Dunarea de Jos" University of Galati, Romania
e-mail: simona_boiciuc@yahoo.com

ABSTRACT

The paper presents the obtaining of thin films out of ZnO by thermal evaporation and oxidation, in a conventional furnace, at various temperatures between 350-550 °C of films from pure Zn deposited. The influence of current intensity, deposition time and oxidation temperature on film structure and transparency was monitored.

KEYWORDS: thermal evaporation of zinc, thermal oxidation

1. Introduction

Obtaining thin films through physical vapor deposition processes aims to achieve superficial properties of electronic, optical, magnetic, thermal, chemical and mechanical nature.

This involves a sequence of stages such as [1, 2]:

- the production in the working space of a flow of atoms or molecules from the target material to the substrate surface;
- the condensation of the flow of atoms or molecules on the surface of the substrate;
- the germination and growth of the layer.

In the case of thermal evaporation, the transfer of the source material in the vapor phase involves heating it to sufficiently high temperatures that its vapor pressure enables acceptable deposition rates to be achieved. In case of deposition of pure metals, it is necessary that the heating temperature of the source material to ensure a vapor pressure of approx. 1.5 Pa.

Molecules condensed and adsorbed to the surface of the substrate undergo a superficial diffusion process that results in putting them in order and the formation of crystallites, or they may undergo a reversible desorption process.

The zinc oxide has different applications in the manufacture of devices such as solar cells, laser diodes, field-emitting devices, chemical and gas sensors (nanostructured ZnO can increase the properties of gas sensors due to a larger and more reactive surface). Its biocompatibility also makes it attractive for biomedical applications. It has antimicrobial, antiseptic properties and can be used to make dentures. It can provide anti-corrosion properties, and by adding to organic coatings it improves adhesion and flexibility, also giving shine (gloss).

The thin films nanostructured by ZnO belong to the category of semiconductor materials, with wide energy band, high optical transparency in the visible field, with high chemical and thermal stability, and electrical conductivity in a wide range of values [3, 4].

It has a density of 5.606 g/cm^3, a melting temperature of 1975 °C, a boiling temperature of 2360 °C, the energy of the forbidden band 3.37 eV, the mobility of electrons at T = 300 K of 200 cm^2/V s, the mobility of the gaps at T = 300K of 5-50 cm^2/V s [5-7].

ZnO crystallizes into a hexagonal network of the wurtzit type, Fig. 1 this structure is described as consisting of a sequence of planes composed of ions of O^{2-} and Zn^{2+}, arranged alternately along the axis of the hexagonal cell C, [5-7].

Within the wurtzite structure considered to be the most stable, the oxygen anions and zinc cations form a tetrahedral unit. The entire structure has no central symmetry.

Regarding the mechanical properties of ZnO, it is a relatively soft material with a hardness of about 4.5 on the Mohs scale. The high thermal and calorific capacity, low thermal expansion and high melting temperature recommend ZnO deposits in many applications [5, 6].

The method of thermal oxidation, used in this work for obtaining ZnO, involves the deposition of layers of pure zinc, by thermal evaporation and their oxidation in air, in a furnace, at different temperatures. The influence of the deposition

THE ANNALS OF "DUNAREA DE JOS" UNIVERSITY OF GALATI
FASCICLE IX. METALLURGY AND MATERIALS SCIENCE
N°. 2 - 2022, ISSN 2668-4748; e-ISSN 2668-4756
Article DOI: https://doi.org/10.35219/mms.2022.2.06

parameters and the oxidation temperature on the characteristics of the films obtained was monitored.

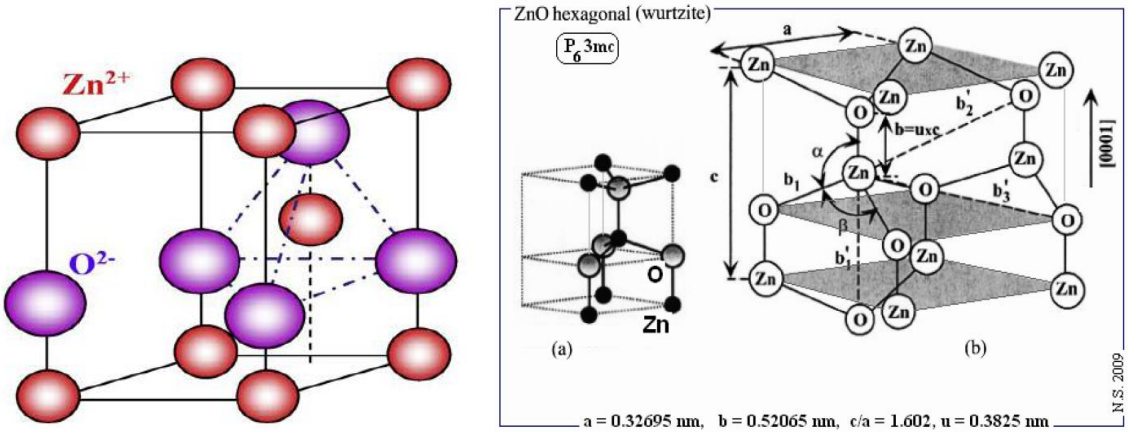

Fig. 1. *Crystalline structure of zinc oxide* [5-7]

2. Experimental conditions

Zinc thin films were deposited on a glass support, by thermal evaporation, the PVD process. For deposits, 99.99% Zn purity target was used.

The pressure in the deposition chamber was in the order of $4*10^{-4}$ Torr. During the deposition process, the glass substrate was kept at the room temperature. The distance between the zinc source and the substrate was of 60 mm. The substrate is rotated continuously to even out the thickness of the deposited film.

In order to obtain quality films, it is important to clean and activate the substrate in order to remove surface impurities, adsorbed gases and to form stable and strong physical and chemical connections between the substrate and the condensed material. In this respect, a chemical cleaning of the substrates was carried out in ultrasonic baths, using 50% ethyl alcohol. The action was carried out at a temperature of 20 °C, for 60 seconds, followed by rinsing with distilled water and drying.

The oxidation of zinc films was achieved by heating at various temperatures between 350 °C – 550 °C, for 600 seconds.

A number of regimes presented in Table 1 were used to obtain the films.

Microscopic analysis of the films obtained was performed using a Neophot 2 optical microscope with computerized data acquisition.

Before and after oxidation, each sample was subjected to transparency measurements.

Film transparency was determined using an electronic apparatus using a light source and photoreceptor. The light after passing through the deposited film is measured by means of the photoreceptor and an amplifier and the result is displayed with an analogue device.

Table 1. *Zinc Films-obtaining regimes*

Sample Code	Current intensity [A]	Deposition time [s]	Oxidation temperature [°C]	Oxidation time [s]
P1	28	2	420	600
P2	28	3	550	600
P3	28	8	380	600
P4	22	3	350	600
P5	24	3	420	600
P6	28	3	550	600

3. Results and Discussion

Analysing Table 1, it can be found that the thermal evaporation deposition process has a short duration due to a high evaporation rate of the target material.

The microscopic analysis performed on the Zn films revealed that they had homogeneous, stable, uniform structures, with a good adhesion to the substrate and without cracks, as can be seen in Figure 2 and Figure 4.

THE ANNALS OF "DUNAREA DE JOS" UNIVERSITY OF GALATI
FASCICLE IX. METALLURGY AND MATERIALS SCIENCE
Nº. 2 - 2022, ISSN 2668-4748; e-ISSN 2668-4756
Article DOI: https://doi.org/10.35219/mms.2022.2.06

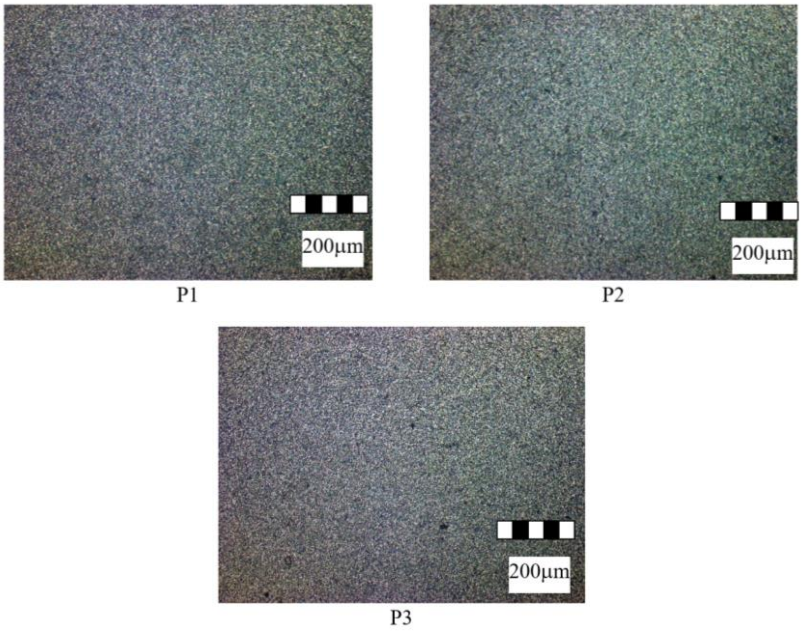

Fig. 2. *Micrographs of Zn films, deposited by thermal evaporation, for samples obtained at different deposition times P1 - 2 s; P2 - 3 s; P3 - 8 s (constant current intensity)*

In the case of thermal evaporation, due to the reduced pressure in the enclosure, the mean free path of the particles is greater than the source-substrate distance and they reach the support with the same energy as they have when passing into the vapor phase. The energy of the thermally evaporated particles is low (0.1-0.4 eV), which makes the flux of condensing atoms on the surface of the support bring a low energy input. This will lead to less compact structures.

The purity of the deposited film depends on the quality of the vacuum and the purity of the target. Collision with waste gases may result in deposits of uneven thickness and impurities.

With the increase of the deposition time, at the same current intensity, there is a slight increase of the granulation, with a tendency of grouping the zinc crystals, Fig. 2.

Following the measurement of the initial transparency of zinc films, P1, P2, P3, a decrease was found with the increase of the deposition time. This is due to the increase in the thickness of the deposited layer, Fig. 3.

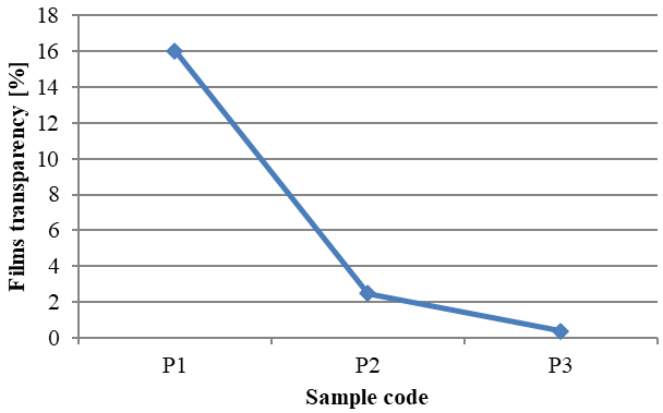

Fig. 3. *The influence of the deposition time on the initial transparency of zinc films for samples P1 - 2 s, P2 - 3 s, P3 - 8 s*

Regarding the influence of the current intensity on the structure of the zinc films deposited, it is found that at lower current intensities there is a tendency to finish the grain (P4, P5).

THE ANNALS OF "DUNAREA DE JOS" UNIVERSITY OF GALATI
FASCICLE IX. METALLURGY AND MATERIALS SCIENCE
No. 2 - 2022, ISSN 2668-4748; e-ISSN 2668-4756
Article DOI: https://doi.org/10.35219/mms.2022.2.06

At the increase of the current intensity, at the same deposition time, there is a tendency to increase the granulation, P6 Fig. 4.

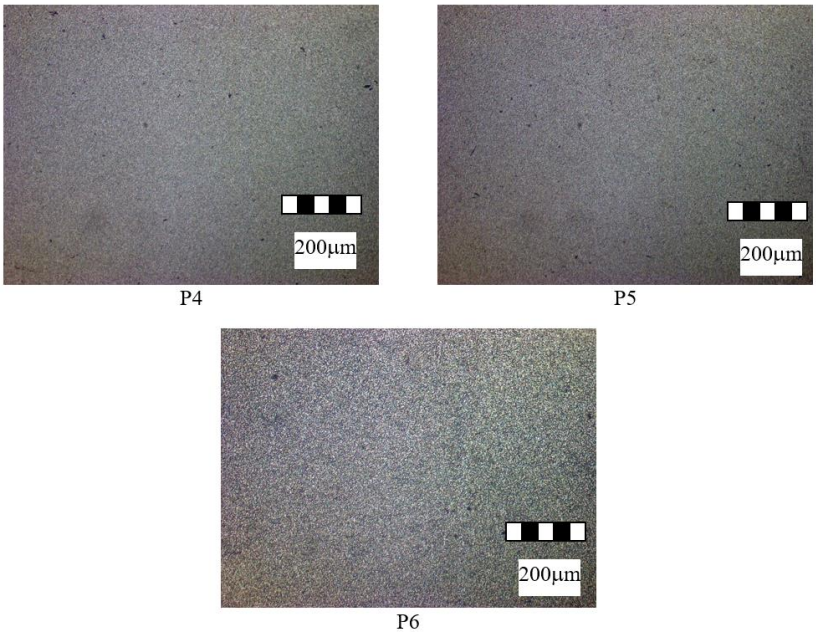

Fig. 4. *Micrographs of Zn films, submitted through thermal evaporation, for samples obtained at different current intensities P4 - 22 A; P5 - 24 A; P6 - 28 A (same deposition time)*

Following the measurement of the initial transparency of the zinc films deposited, a decrease of the transparency at the same time as the increase of the current intensity was found. This is due to the increase in the thickness of the deposited layer, as a result of the intensification of the evaporation - Fig. 5.

The colour of the zinc films deposited is metallic grey and after oxidation in air at different temperatures it becomes lighter as the thickness of the deposition is lower, which indicates the formation of ZnO.

The microscopic analysis performed on Zn films subjected to oxidation at different temperatures, Fig. 6, highlights a slight increase in granulation with the oxidation temperature.

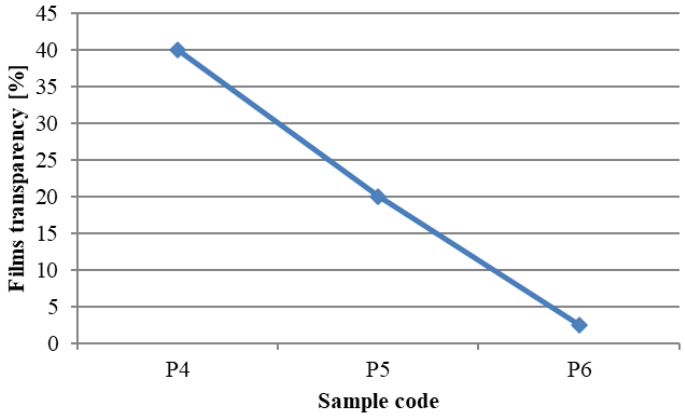

Fig. 5. *Influence of current intensity on the initial transparency of zinc films for samples P4 - 22 A; P5 - 24 A; P6 - 28 A*

THE ANNALS OF "DUNAREA DE JOS" UNIVERSITY OF GALATI
FASCICLE IX. METALLURGY AND MATERIALS SCIENCE
Nº. 2 - 2022, ISSN 2668-4748; e-ISSN 2668-4756
Article DOI: https://doi.org/10.35219/mms.2022.2.06

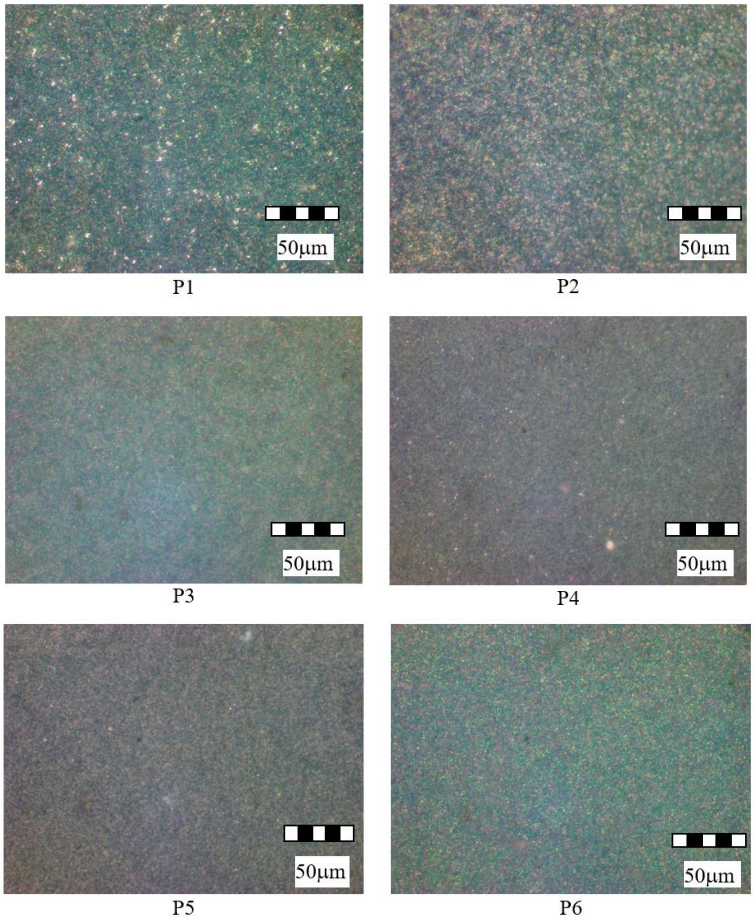

Fig. 6. *Micrographs of ZnO films oxidized at different temperatures*

Table 2. *Transparency of the films*

Sample Code	Final transparency [%]
P1	58.8
P2	62.5
P3	55.5
P4	97
P5	80
P6	62.5

With the increase of the oxidation temperature, the transparency of the films increases, which indicates the formation of ZnO (in accordance with the thicknesses obtained), Table 2.

4. Conclusions

Following the experimental researches carried out, the following conclusions can be highlighted:

- obtaining films of ZnO through thermal evaporation and oxidation in air at various temperatures is a fairly commonly used, economical and non-polluting method;
- low melting point metals may be deposited;
- the pressure in the chamber influences the kinetic energy of the atoms upon their arrival on the substrate, thus influencing the structure of the deposited layer, the density and the porosity;
- a high correlation of deposition parameters is required; their possible variations during the process may lead to non-homogeneities in the chemical composition and crystalline structure of the film; surface irregularities may cause shading effects;
- due to the low energy of the thermally evaporated particles, the deposited films may have a higher porosity and lower density;
- from a structural point of view, the films obtained are uniform, adherent and free from cracks;
- the structure and transparency of the films are influenced by the deposition parameters: the transparency of the films made of Zn decreases with the increase of the deposition time and the intensity of the current due to the increase of the coating thickness;

- transparency of ZnO films increases with increasing oxidation temperature.

References

[1]. Viorica Muşat, *Filme subţiri multifuncţionale*, Editura CERMI Iaşi, 20, p. 33-59, 2005.
[2]. Vermeşan G., Vermeşan E., *et al.*, *Introducere în ingineria suprafeţelor*, Editura Dacia Cluj Napoca, 1999.
[3]. Animesh Kumar Singh, Radhakanta Kishan, *Comparative Study of Zinc Oxide Nanostructures Synthesized by Oxidization of Zinc Foil and Zinc Powder*, Department of Metallurgical & Materials Engineering, National Institute of Technology, Rourkela, Deemed University, 2011.
[4]. Zhiyong Fan, Jia G. Lu, *Zinc Oxide Nanostructures: Synthesis and Properties*, Department of Chemical Engineering and Materials Science & Department of Electrical Engineering and Computer Science, University of California, Irvine, CA 92697, USA, 2005.
[5]. Orathai Yawong, Supab Choopun, **Pongsri Mangkorntong, Nikorn Mangkorntong**, *Zinc Oxide Nanostructure by Oxidization of Zinc Thin Films*, CMU. Journal Special Issue on Nanotechnology, vol. 4(1), 2005.
[6]. Manish Kumar, Shakti Swarup Sahu, *Zinc Oxide Nanostructures Synthesized by Oxidization of Zinc*, Dept. of Metallurgical & Materials Engineering, National Institute of Technology, Rourkela Rourkela, Orissa, 2010.
[7]. Ozgur U., Alivov Y. I., Liu C., Teke A., Reschikov M. A., Dogan S., Avrutin V., Cho S.-J., Morkoc H., *A comprehesive review of ZnO materials and devices*, Journal of Applied Physics, 98, 041301, 2005.

THE ANNALS OF "DUNAREA DE JOS" UNIVERSITY OF GALATI
FASCICLE IX. METALLURGY AND MATERIALS SCIENCE
Nº. 2 - 2022, ISSN 2668-4748; e-ISSN 2668-4756
Article DOI: https://doi.org/10.35219/mms.2022.2.07

EQUILIBRIUM STUDY REGARDING CRYSTAL VIOLET DYE ADSORPTION ON RASPBERRY LEAVES POWDER

Giannin MOSOARCA[1], Cosmin VANCEA[1], Simona POPA[1], Sorina BORAN[1], Maria Elena RADULESCU-GRAD[2]

[1]Faculty of Industrial Chemistry and Environmental Engineering, Politehnica University Timisoara, Romania
[2]"Coriolan Dragulescu" Institute of Chemistry, Romanian Academy, Timisoara, Romania
e-mail: giannin.mosoarca@upt.ro

ABSTRACT

This work focuses on the crystal violet removal from aqueous solution using raspberry leaves powder as adsorbent materials. SEM and colour analyses were used to characterize the adsorbent surface. The influence of pH, adsorbent dose and initial dye concentration was studied. Equilibrium modeling was performed to characterize the adsorption process and to determine the maximum adsorption capacity. Sips isotherm characterizes the adsorption and the maximum adsorption capacity, 264.5 (mg/g) was better compared with other similar adsorbents. The obtained results indicate that adsorbent material, obtained from raspberry leaves, is very suitable to be used for crystal violet removal from aqueous solutions.

KEYWORDS: dye adsorption, crystal violet, raspberry leaves, equilibrium isotherms

1. Introduction

Dyes are a major class of compounds that, once in the environment, can cause environmental imbalances. The main sources of dye pollution are wastewater from the textile, cosmetics, food, pharmaceuticals, paper and printing industries. If they are not treated properly, their discharge into natural effluents can have negative effects on aquatic fauna and flora [1-4].

Crystal violet is a dye with many industrial applications and also, in veterinary medicine. It has a toxic, carcinogenic and mutagenic potential on human health and the environment [3, 5, 6].

Various methods have been studied and applied to remove this dye from water such as: photo-catalytic degradation, membrane separation, catalytic reduction, chemical electrochemical oxidation, adsorption, microorganism degradation and biological treatment [2, 4, 6-8].

Adsorption is a preferred applied method in many cases because it is easy to operate, it has a good applicability and flexibility, high efficiency and relatively low costs [1-4, 8].

The use of cheap and available in large quantities adsorbent materials can make this process extremely cost-effective from an economic point of view [2-4].

This category includes vegetable waste such as: various seeds, leaves, steams, peels and husks [1-5, 8, 9].

Raspberry (*Rubus idaeus*) is a shrub that grows spontaneously or is widely grown in temperate areas of Europe, Asia and North America. Its fruits are appreciated for their taste and contain high amounts of vitamins, minerals, organic acids, tannins and flavonoids. These characteristics make raspberries to be used in the food, cosmetics and pharmaceutical industries [10-12]. The leaves of this shrub are available in large quantities in nature and have low cost.

The main aim of this study was to use this vegetable product to remove the crystal violet from aqueous solutions. Obtaining the adsorbent material from the raspberry leaves required minimal processing, without using chemical reagents and without heat treatment. Equilibrium modeling was performed to characterize the adsorption process and to determine the maximum adsorption capacity. It was compared with those obtained for other similar adsorbent materials used to remove the crystal violet dye from water.

THE ANNALS OF "DUNAREA DE JOS" UNIVERSITY OF GALATI
FASCICLE IX. METALLURGY AND MATERIALS SCIENCE
N°. 2 - 2022, ISSN 2668-4748; e-ISSN 2668-4756
Article DOI: https://doi.org/10.35219/mms.2022.2.07

2. Experimental

The dried raspberry leaves were purchased from StefMar, Ramnicu Valcea. The adsorbent obtaining process (which involves grinding and washing) has been described in detail elsewhere [13].

To characterize the adsorbent surface, SEM and color analyzes were performed using a Quanta FEG 250 microscope and a Cary-Varian 300 Bio UV-VIS colorimeter (D65 illuminant), respectively.

All experiments were performed in three independent replicates, at constant mixing intensity. The pH was adjusted with NaOH (0.1 N) and HCl (0.1 N) solutions and the crystal violet concentration was determined using a UV-VIS spectrophotometer (Specord 200 PLUS) at 590 nm.

The adsorption capacity at equilibrium, (qe), was calculated with equation (1):

$$q_e = \frac{(C_0 - C_e)\cdot V}{m} \quad (1)$$

where: C_0 represents the initial crystal violet concentration (mg/L); C_e represents the crystal violet equilibrium concentration (mg/L); V represents the solution volume (L) and m represents the mass of adsorbent (g).

Langmuir, Freundlich, Temkin and Sips isotherms in the non-linear forms (equations 2-5) were used to analyse the adsorption equilibrium.
Langmuir isotherm equation:

$$q_e = \frac{q_m \cdot K_L \cdot C_e}{1 + K_L \cdot C_e} \quad (2)$$

Freundlich isotherm equation:

$$q_e = K_F \cdot C_e^{1/n_F} \quad (3)$$

Temkin isotherm equation:

$$q_e = \frac{R \cdot T}{b} \cdot \ln(K_T \cdot C_e) \quad (4)$$

Sips isotherm equation:

$$q_e = \frac{Q_{sat} \cdot K_S \cdot C_e^n}{1 + K_S \cdot C_e^n} \quad (5)$$

where: q_m and Q_{sat} represents the maximum absorption capacities; K_L represents the Langmuir constant, K_F represents the Freundlich constant, K_T represents the Temkin constant, K_S represents the Sips constant; $1/n_F$ represents an empirical constant indicating the intensity of adsorption; R represents the universal gas constant; T represents the absolute temperature; b represents Temkin constant which related to the adsorption heat and n represents Sips isotherm exponent [14-16].

3. Results and Discussion

3.1. Adsorbent surface characterization

Figure 3 shows the SEM images (at 800 X) of adsorbent surface, before and after adsorption. Before adsorption (Figure 1A), the surface is irregular and uneven, with trichomes specific to raspberry leaves. These specific formations have been (identified) emphasized in other studies that have analysed the SEM images of raspberry leaves [11].

After adsorption (Figure 1B), the surface morphology is modified. The surface of the dye-loaded adsorbent presents compact structure. Homogeneity and smoothness of the surface is due to the retained dye molecules, indicating that adsorption had occurred at the material surface.

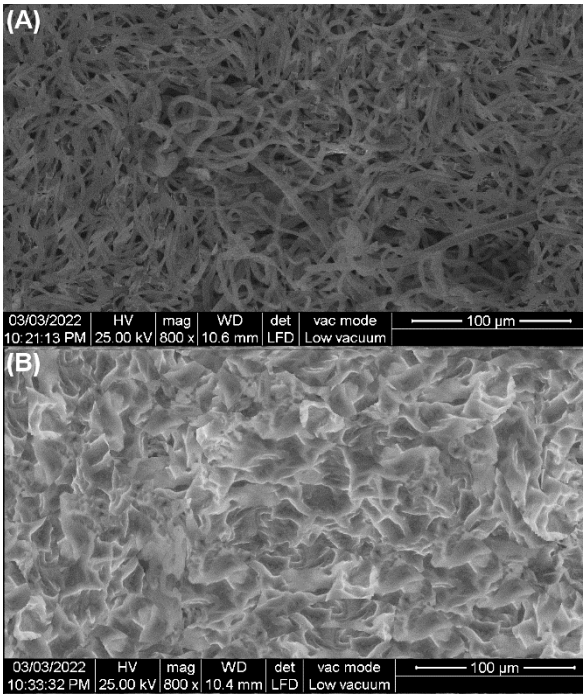

Fig. 1. *SEM images of adsorbent surface before (A) and after (B) adsorption*

Colour analysis in the *CIEL*a*b** system was used to characterize the colour of the adsorbent, before and after desorption (Figure 2).

Before adsorption, the colour of the adsorbent material is described by point 1 and after adsorption

THE ANNALS OF "DUNAREA DE JOS" UNIVERSITY OF GALATI
FASCICLE IX. METALLURGY AND MATERIALS SCIENCE
Nº. 2 - 2022, ISSN 2668-4748; e-ISSN 2668-4756
Article DOI: https://doi.org/10.35219/mms.2022.2.07

by point 3. The crystal violet dye colour is described point 2. After adsorption, a change in the value of the colour parameters (*L**, *a**, *b**) is observed, which indicates the change of the adsorbent colour, point 3 being found in the colour quarter of crystal violet.

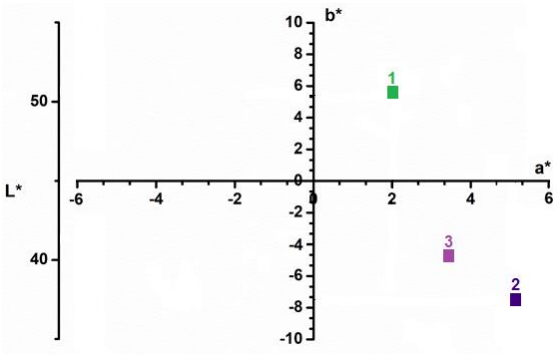

Fig. 2. CIEL*a*b* *colour parameters: 1- raspberry leaves powder; 2 - crystal violet dye; 3 - raspberry leaves powder after adsorption*

3.2. Influence of solution pH on adsorption capacity

The point of zero charge (pH_{PZC}) indicates when the adsorbent surface is positively or negatively charged depending on the pH. The pH_{PZC} of adsorbent materials was previously determined as 5.6 [13].

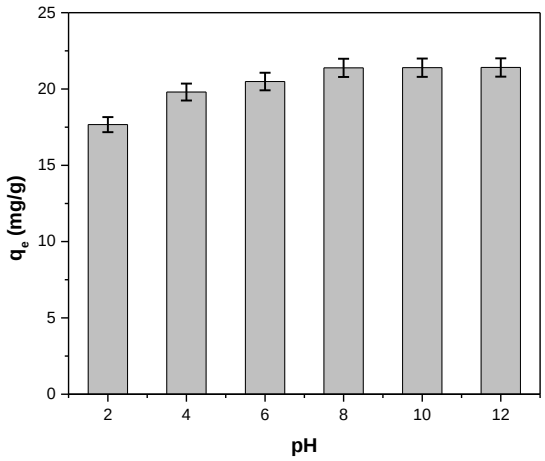

Fig. 3. *The influence of solution pH on adsorption capacity*

Figure 3 illustrate the influence of pH solution on the adsorption. The value of this parameter increases with the increasing of the pH. A similar observation was mentioned in other previous studies regarding the crystal violet dye adsorption of similar adsorbents obtained from vegetal wastes [4, 9, 17-19]. At lower pH values than pH_{PZC} (5.6) the adsorbent surface is positive charge and electrostatic repulsion occurs between cationic dye and raspberry leaves powder. At higher pH values than pH_{PZC} the adsorbent surface is negative and electrostatic attraction favours the process [9, 15, 19].

3.3. Influence of adsorbent dose on adsorption capacity

The adsorbent dose influence on adsorption capacity is shown in Figure 4. The increase of adsorbent dose has a negative effect on the adsorption capacity. A similar behavior was observed at crystal violet adsorption on *Ocotea puberula* bark powder [9], *Terminalia arjuna sawdust* [2], *Eragrostis plana Nees* [16], *Moringa oleifera* pod husk [17], coniferous pinus bark powder [20], rice bran [21], wheat bran [21] and corn stalk [22] and lilac tree leaves powder [23]. When the adsorbent dose increases, the available adsorption sites number increases, but many remain unsaturated. Agglomeration and aggregation of adsorbent material particles may occur at high adsorbent dose. This phenomenon's led to a decrease in the adsorption capacity [2, 21-23].

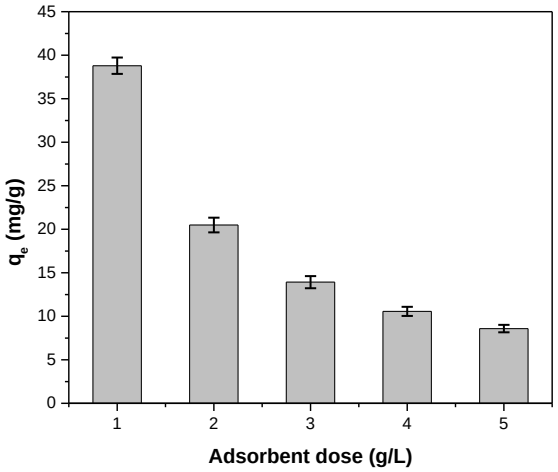

Fig. 4. *The influence of adsorbent dose on adsorption capacity*

3.4. Influence of initial dye concentration on adsorption capacity

The adsorption capacity is significantly influenced by the increase of the initial dye concentration. The positive effect is explained by the fact that the increase of the initial concentration of the dye favours the number of collisions between the dye and adsorbent molecules. At the same time, it increases the driving force required to overcome the mass transfer resistance of the dye from solution on the adsorbent surface [2, 4, 16, 17, 23].

THE ANNALS OF "DUNAREA DE JOS" UNIVERSITY OF GALATI
FASCICLE IX. METALLURGY AND MATERIALS SCIENCE
No. 2 - 2022, ISSN 2668-4748; e-ISSN 2668-4756
Article DOI: https://doi.org/10.35219/mms.2022.2.07

The same variation of the adsorption capacity with the initial dye concentration was reported to the crystal violet adsorption on *Terminalia arjuna* sawdust [2], cedar cone [4], *Ocotea puberula* bark [9], *Moringa oleifera* pod husk [17], *Punica granatum* shell [19] and corn stalk [22], lilac tree leaves powder [23], jackfruit leaf powder [24] and pineapple leaf powder [25].

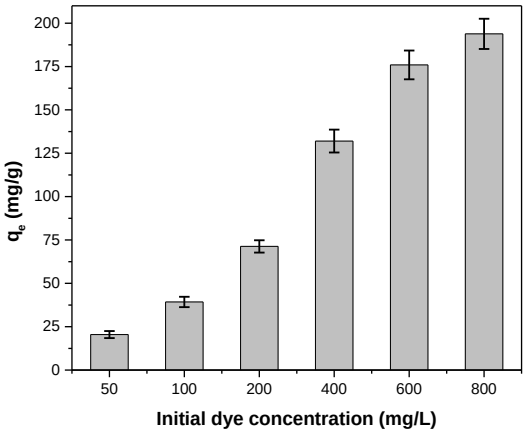

Fig. 5. *The influence of initial dye concentration on adsorption capacity*

The changes of the surface morphology and the adsorbent material colour, highlighted by the SEM and colour analyses, as well as the experimentally obtained values for the adsorption capacity demonstrate the affinity of raspberry powder for the violet crystal dye retention.

3.5. Adsorption isotherms

In order to study the equilibrium adsorption four isotherm were tested to fit the experimental data: Langmuir, Freundlich, Temkin and Sips. The isotherms curves for crystal violet dye adsorption are presented in Figures 6-9. The adsorption isotherms constants are shown in Table 1.

In order to establish the most suitable model that characterizes the adsorption process, the values obtained for determination coefficient (R^2), chi-square (χ^2) and average relative error (ARE) were taken into account.

$$R^2 = 1 - \frac{\sum_{i=1}^{n}\left(y_{i,exp} - y_{i,mod}\right)^2}{\sum_{i=1}^{n}\left(y_{i,exp} - \overline{y_{i,exp}}\right)^2} \quad (6)$$

$$\chi^2 = \sum_{i=1}^{n}\frac{\left(y_{i,exp} - y_{i,mod}\right)^2}{y_{i,mod}} \quad (7)$$

$$ARE = \frac{100}{n}\sum_{i=1}^{n}\left|\frac{y_{i,exp} - y_{i,mod}}{y_{i,mod}}\right| \quad (8)$$

where: $y_{i,exp}$ represents the experimental value; $y_{i,mod}$ represents the modeled value; $\overline{y_{i,exp}}$ represents the mean values and n is the total amount of information [14].

Analysing the obtained data, it can be concluded that the Sips isotherm best described the crystal violet adsorption process on raspberry leaves powder (the higher value of R^2 and the lowest values for χ^2 and ARE).

The value of the maximum adsorption capacity obtained for the adsorbent material is higher compared to that of other similar adsorbents used for the retention of crystal violet.

Table 2 presents comparatively the maximum adsorption capacities values for several similar adsorbents.

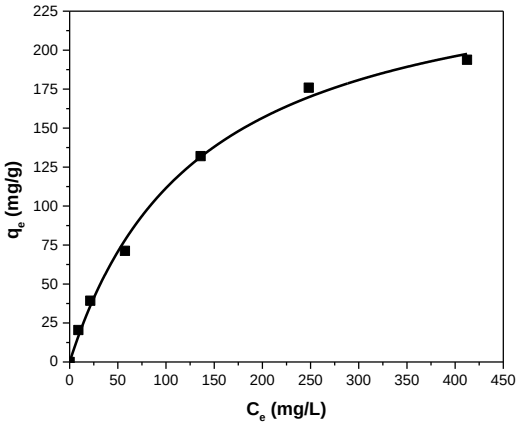

Fig. 6. *Langmuir isotherm for crystal violet adsorption on raspberry leaves powder*

THE ANNALS OF "DUNAREA DE JOS" UNIVERSITY OF GALATI
FASCICLE IX. METALLURGY AND MATERIALS SCIENCE
No. 2 - 2022, ISSN 2668-4748; e-ISSN 2668-4756
Article DOI: https://doi.org/10.35219/mms.2022.2.07

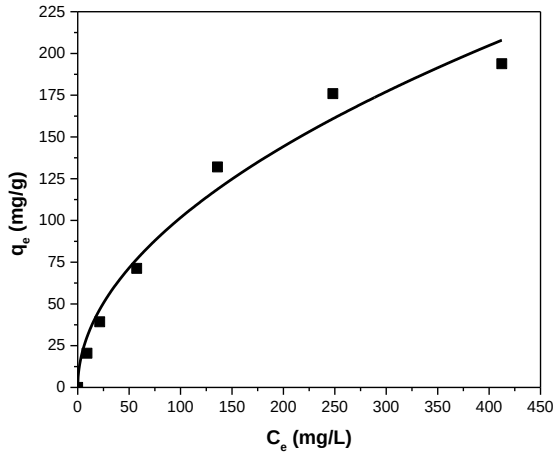

Fig. 7. *Freundlich isotherm for crystal violet adsorption on raspberry leaves powder*

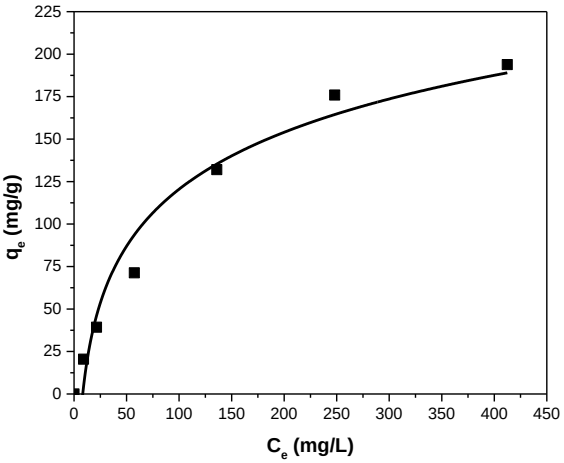

Fig. 8. *Temkin isotherm for crystal violet adsorption on raspberry leaves powder*

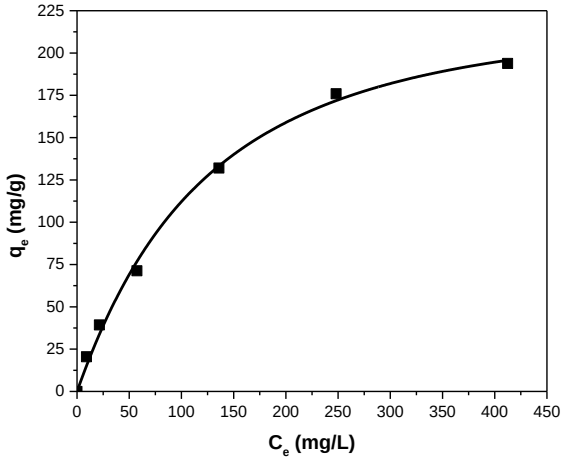

Fig. 9. *Sips isotherm for crystal violet adsorption on raspberry leaves powder*

Table 1. *The adsorption isotherms constants*

Isotherm model	Parameters	Value
Langmuir	K_L (L/mg)	0.007 ± 0.001
	q_{max} (mg/g)	262.4 ± 6.38
	R^2	0.995
	χ^2	2.22
	ARE (%)	6.97
Freundlich	K_f (mg/g)	9.92 ± 0.83
	1/n	0.50 ± 0.05
	R^2	0.978
	χ^2	8.54
	ARE (%)	11.79
Temkin	K_T (L/mg)	0.123 ± 0.042
	b (kJ/g)	50.55 ± 4.69
	R^2	0.972
	χ^2	70.69
	ARE (%)	62.75
Sips	Q_{sat} (mg/g)	264.5 ± 8.25
	K_S (L/mg)	0.007 ± 0.001
	n	0.99 ± 0.09
	R^2	0.997
	χ^2	2.07
	ARE (%)	6.65

Table 2. *Maximum adsorption capacities values of similar adsorbent materials used for the crystal violet dye removal from aqueous solutions*

Adsorbent material	Maximum adsorption capacity (mg/g)	Reference
water hyacinth root powder	322.58	[26]
raspberry leaves powder	**264.5**	**This study**
grapefruit peel	254.16	[28]
common lilac tree leaves powder	196.75	[23]
Moringa oleifera pod husk	156.25	[17]
wood apple shell	129.87	[18]
wheat bran	69.15	[21]
coir pith	65.53	[15]
Punica granatum shell	50.21	[19]
jackfruit leaf powder	43.39	[24]
rice bran	41.68	[21]
pinus bark powder	32.78	[20]
cedar cones	13.64	[4]
almond shells	12.20	[8]
corn stalk	9.64	[22]
pineapple crown leaves	6.49	[29]

THE ANNALS OF "DUNAREA DE JOS" UNIVERSITY OF GALATI
FASCICLE IX. METALLURGY AND MATERIALS SCIENCE
N°. 2 - 2022, ISSN 2668-4748; e-ISSN 2668-4756
Article DOI: https://doi.org/10.35219/mms.2022.2.07

The possibility of regeneration of the exhausted adsorbent was achieved using three desorption reagents: HCl (0.1 N), NaOH (0.1 N) and distilled water. The efficiency of the desorption process was less than 30% for all desorption agents tested. Based on these results and taking into account the fact that the raspberry leaves are a cheap material, easily accessible and available in large quantities, it can be concluded that regeneration is not rentable.

Based on its combustion properties the adsorbent resulting from adsorption can be incinerated in specialized incinerators. Another option is to be used as a porogenous agent for obtaining cellular glass and porous ceramic materials, due to the resulted gases in the thermal synthesis process of these products.

4. Conclusions

The adsorption capacity of the adsorbent material obtained from raspberry leaves is influenced by pH, adsorbent dose and initial dye concentration.

Sips isotherm best described the crystal violet adsorption. The obtained maximum adsorption capacity, 264.5 (mg/g) was higher compared to other similar adsorbents obtained from vegetal wastes.

The results of this study indicate that the raspberry leaves powder is very suitable for crystal violet adsorption from aqueous solutions.

References

[1]. Pang X., Sellaoui L., Franco D., Dotto G. L., Georgin J., Bajahzar A., Belmabrouk H., Ben Lamine A., Bonilla-Petriciolet A., Lia Z., *Adsorption of crystal violet on biomasses from pecan nutshell, para chestnut husk, araucaria bark and palm cactus: Experimental study and theoretical modeling via monolayer and double layer statistical physics models*, Chemical Engineering Journal, 378, 122101, 2019.

[2]. Shakoor S., Nasar, A., *Adsorptive decontamination of synthetic wastewater containing crystal violet dye by employing Terminalia arjuna sawdust waste*, Groundwater for Sustainable Development, 7, p. 30-38, 2018.

[3]. Shoukat S., Bhatti H. N., Iqbal M., Noreen, S., *Mango stone biocomposite preparation and application for crystal violet adsorption: A mechanistic study*, Microporous and Mesoporous Materials, 239, p. 180-189, 2017.

[4]. Zamouche M., Habib A., Saaidia K., Lehocine M. B., *Batch mode for adsorption of crystal violet by cedar cone forest waste*, SN Applied Sciences, 2, 198, 2020.

[5]. Chahinez H.O., Abdelkader O., Leila Y., Tran H. N., *One-stage preparation of palm petiole-derived biochar: Characterization and application for adsorption of crystal violet dye in water*, Environmental Technology & Innovation, 19, 100872, 2020.

[6]. Franco D. S. P., Fagundes J. L. S., Georgin J., Salaua N. P. G., Dotto G. L., *A mass transfer study considering intraparticle diffusion and axial dispersion for fixed-bed adsorption of crystal violet on pecan pericarp (Carya illinoensis)*, Chemical Engineering Journal, 397, 125423, 2020.

[7]. Kosar Hashemi Y., Tavakkoli Yaraki M., Ghanbari S., Heidarpoor Saremi L., Givianrad M. H., *Photodegradation of organic water pollutants under visible light using anatase F, N co-doped TiO_2/SiO_2 nanocomposite: Semi-pilot plant experiment and density functional theory calculations*, Chemosphere, 275, 129903, 2021.

[8]. Loulidi I., Boukhlifi F., Ouchabi M., Amar A., Jabri M., Kali A., Chraibi S., Hadey C., Aziz F., *Adsorption of crystal violet onto an agricultural waste residue: kinetics, isotherm, thermodynamics and mechanism of adsorption*, The Scientific World Journal, 2020, 5873521, 2020.

[9]. Georgin J., Franco D. S. P., Netto M. S., Allasia D., Oliveira M. L. S., Dotto G. L., *Evaluation of Ocotea puberula bark powder (OPBP) as an effective adsorbent to uptake crystal violet from colored effluents: Alternative kinetic approaches*, Environmental Science and Pollution Research, 27, p. 25727-25739, 2020.

[10]. Chevallier A., *Encyclopedia of Herbal Medicine: 550 Herbs and Remedies for Common Ailments*, 3rd ed., DK Publishing: New York, NY, USA, p. 264, 2016.

[11]. Chwil M., Kostryco M., *Histochemical assays of secretory trichomes and the structure and content of mineral nutrients in Rubus idaeus L. leaves*, Protoplasma, 257, p. 119-139, 2020.

[12]. Yang Y., Yin X., Zhang D., Lu J., Wang X., *Isolation, Structural Characterization and Macrophage Activation Activity of an Acidic Polysaccharide from Raspberry Pulp*, Molecules, 27, 1674, 2022.

[13]. Mosoarca G., Popa S., Vancea C., Dan M., Boran S., *Removal of Methylene Blue from Aqueous Solutions Using a New Natural Lignocellulosic Adsorbent - Raspberry (Rubus idaeus) Leaves Powder*, Polymers, 14, 1966, 2022.

[14]. Piccin J. S., Cadaval T. R. S., de Pinto L. A. A., Dotto G. L., *Adsorption isotherms in liquid phase: Experimental, modeling and interpretations*, In: *Adsorption Processes for Water Treatment and Purification*, Bonilla-Petriciolet A., Mendoza-Castillo D., Reynel-Avila H. (Eds.), Springer, Switzerland, p. 19-51, 2017.

[15]. Fabryanty R., Valencia C., Soetaredjo F. E., Putro J. N., Santoso S.P., Kurniawan A., Ju Y. H., Ismadji S., *Removal of crystal violet dye by adsorption using bentonite - alginate composite*, Journal of Environmental Chemical Engineering, 5(6), p. 5677-5687, 2017.

[16]. Filho A. C. D., Mazzocato A. C., Dotto G. L., Thue P. S., Pavan F. A., *Eragrostis plana Nees as a novel eco-friendly adsorbent for removal of crystal violet from aqueous solutions*, Environmental Science and Pollution Research, 24, p. 19909-19919, 2017.

[17]. Keereerak A., Chinpa W., *A potential biosorbent from Moringa oleifera pod husk for crystal violet adsorption: Kinetics, isotherms, thermodynamic and desorption studies*, Science Asia, 46, p. 186-194, 2020.

[18]. Jain S., Jayaram R. V., *Removal of basic dyes from aqueous solution by low-cost adsorbent: Wood apple shell (Feronia acidissima)*, Desalination, 250(3), p. 921-927, 2010.

[19]. Silveira M. B., Pavan F. A., Gelos N. F., Lima E. C., Dias S. L., *Punica granatum shell preparation, characterization, and use for crystal violet removal from aqueous solution*, *Clean-Soil Air Water*, 42(7), p. 939-946, 2014.

[20]. Ahmad R., *Studies on adsorption of crystal violet dye from aqueous solution onto coniferous pinus bark powder (CPBP)*, Journal of Hazardous Materials, 171, p. 767-773, 2009.

[21]. Wang X. S., Liu X., Wen L., Zhou Y., Jiang Y., Li Z., *Comparison of Basic Dye Crystal Violet Removal from Aqueous Solution by Low-Cost Biosorbents*, Separation Science and Technology, 43, p. 3712-3731, 2008.

[22]. Muhammad U. L., Zango Z. U., Kadir H. A., Usman A., *Crystal violet removal from aqueous solution using corn stalk bio-sorbent*, Science World Journal, 14, p. 133-138, 2019.

[23]. Mosoarca G., Vancea C., Popa S., Boran S., *Optimization of crystal violet adsorption on common lilac tree leaf powder as natural adsorbent material*, Global NEST Journal, 24(1), p. 87-96, 2022.

[24]. Saha P. D., Chakraborty S., Chowdhury S., *Batch and continuous (fixed-bed column) bisorption of crystal violet by Artocarpus heterophyllus (jackfruit) leaf powder*, Colloids and Surfaces B: Biointerfaces, 92, p. 262-270, 2012.

[25]. Chakraborty S., Chowdhury S., Saha P. D., *Insight into biosorption equilibrium, kinetics and thermo-dynamics of crystal violet onto Ananas comosus (pineapple) leaf powder*, Applied Water Science, 2, p. 135-141, 2012.

[26]. Kulkarni M. R., Revanth T., Anirudh A., Bhat P., *Removal of crystal violet dye from aqueous solution using water hyacinth: equilibrium, kinetics and thermodynamics study*, Resource-Efficient Technologies, 3(1), p. 71-77, 2017.

[28]. Saeed A., Sharif M., Iqbal M., *Application potential of grapefruit peel as dye sorbent: kinetics, equilibrium and mechanism of crystal violet adsorption*, Journal of Hazardous Materials, 179(1-3), p. 564-572, 2010.

[29]. Nieva A. D., Avena L. G. S., Pascual M. A. M., Pamintuan K. R. S., *Characterization of Powdered Pineapple (Ananas comosus) Crown Leaves as Adsorbent for Crystal Violet in Aqueous Solutions*, IOP Conf. Series: Earth and Environmental Science, 563, 012010, 2020.

MANUSCRISELE, CĂRŢILE ŞI REVISTELE PENTRU SCHIMB, PRECUM ŞI ORICE CORESPONDENŢE SE VOR TRIMITE PE ADRESA:

MANUSCRIPTS, REVIEWS AND BOOKS FOR EXCHANGE COOPERATION, AS WELL AS ANY CORRESPONDANCE WILL BE MAILED TO:

LES MANUSCRIPTS, LES REVUES ET LES LIVRES POUR L'ECHANGE, TOUT AUSSI QUE LA CORRESPONDANCE SERONT ENVOYES A L'ADRESSE:

MANUSCKRIPTEN, ZIETSCHRITFTEN UND BUCHER FUR AUSTAUCH SOWIE DIE KORRESPONDENZ SID AN FOLGENDE ANSCHRIFT ZU SEDEN:

After the latest evaluation of the journals by the National Center for Science Policy and Scientometrics (**CENAPOSS**), in recognition of its quality and impact at national level, the journal will be included in the B^+ category, 215 code (http://cncsis.gov.ro/userfiles/file/CENAPOSS/Bplus_2011.pdf).

The journal is already indexed in:
DOAJ: https://doaj.org/
SCIPIO-RO: http://www.scipio.ro/web/182206
EBSCO: http://www.ebscohost.com/titleLists/a9h-journals.pdf
Google Academic: https://scholar.google.ro
Index Copernicus: https://journals.indexcopernicus.com
Crossref: https://search.crossref.org/

The papers published in this journal can be viewed on the website: http://www.gup.ugal.ro/ugaljournals/index.php/mms

Name and Address of Publisher:
Contact person: Prof. Dr. Eng. Elena MEREUȚĂ
Galati University Press - GUP
47 Domneasca St., 800008 - Galati, Romania
Phone: +40 336 130139
Fax: +40 236 461353
Email: gup@ugal.ro

Name and Address of Editor:
Ș. L. Dr. Eng. Marius BODOR
"Dunarea de Jos" University of Galati, Faculty of Engineering
111 Domneasca St., 800201 - Galati, Romania
Phone: +40 336 130208
Phone/Fax: +40 336 130283
Email: marius.bodor@ugal.ro

AFFILIATED WITH:

- THE ROMANIAN SOCIETY FOR METALLURGY
- THE ROMANIAN SOCIETY FOR CHEMISTRY
- THE ROMANIAN SOCIETY FOR BIOMATERIALS
- THE ROMANIAN TECHNICAL FOUNDRY SOCIETY
- THE MATERIALS INFORMATION SOCIETY (ASM INTERNATIONAL)

Edited under the care of the FACULTY OF ENGINEERING

Annual subscription (4 issues per year)

Fascicle DOI: https://doi.org/10.35219/mms

Volume DOI: https://doi.org/10.35219/mms.2022.2

Editing date: 15.06.2022
Number of issues: 200
Printed by Galati University Press (accredited by CNCSIS)
47 Domneasca Street, 800008, Galati, Romania